Chapter 7

The RAPTOR code for simulating profile dynamics

7.1   Introduction

The problem of profile transport and control was described in detail in the previous chapter. At the end of the chapter, a motivation was given for using a simplified transport code which contains only the essential physics to solve problems where rapid profile evolution is required. The RAPTOR (RApid Plasma Transport simulatOR) code was developed with this aim in mind: to provide a lightweight, simplified transport physics code, sufficiently fast to run very rapidly, including in real-time, yet sufficiently complex to contain the most important physics. As such, the RAPTOR code is much simpler and contains less physics than existing transport codes such as ASTRA and CRONOS. However by making the right choices of which physics to simplify, results comparable to these heavier codes have been obtained.

   This chapter describes the main assumptions of the reduced physics model in Section 7.2. Information on the spatial discretization method used to discretize the equations is given in Section 7.3. As with many transport codes, RAPTOR can be used either in interpretative or in predictive code, and these two modes are described in Sections 7.4 and 7.5, respectively. The latter section also describes a unique feature of RAPTOR, namely that it returns not only the profile evolution but also the sensitivity of the profile evolution to a chosen set of parameters. This chapter is concluded, in Section 7.6, with an outlook on possible extensions of the RAPTOR model and code.

7.1.1   Relation to previous work

In (Witrant et al. 2007), a control-oriented model was introduced to model the poloidal flux and temperature profile. The model used in this thesis is, to some extent, similar to that model, but differs importantly in the modeling of the electron temperature profile. In the model from (Witrant et al. 2007) the T_e profile shape is parametrized with a set of 3 parameters, which are then each derived from global scaling laws; whereas the approach presented in this thesis solves directly the diffusion equation for T_e including a spatially dependent model of electron energy diffusivity that depends directly on magnetic shear and safety factor profiles. It imposes no restrictuions on the T_e profile and

allows extension to more complex transport models. This is more realistic in the case of advanced scenarios with locally improved confinement and transport barriers. Moreover, the numerical scheme used to solve the coupled PDEs is different: finite differences and a mixed implicit-explicit integration method are used in (Witrant et al. 2007), compared to finite elements and a fully implicit method in the present work.

7.2 Reduced physics model

The RAPTOR code in its present form solves the 1D profile diffusion equations (6.26) and(6.53) for $\psi(\rho, t)$ and $T_e(\rho, t)$. The other kinetic profiles T_i, n_e and n_i are kept fixed. The reason for this choice is that the most important nonlinear coupling between plasma profiles during a tokamak discharge stems from the electron temperature-dependent resistivity and bootstrap current and the q profile-dependent confinement. What is more, actuators for temperature and current density are quite effective while the shape of the density profile is, in practice, less well controlled and globally follows a pre-defined evolution during a given discharge (sometimes under feedback control of particle injection/exhaust systems). Still, several more assumptions are made to yield a reduced model for the ψ and T_e profile evolution; these will be discussed below.

7.2.1 Fixed equilibrium assumption

As explained in Section 6.6, the standard practice in 1.5D transport codes is to simultaneously evolve the 1D profiles and the 2D Grad-Shafranov equilibrium. An important simplification used in the RAPTOR code is to not evolve the 2D equilibrium, but to assume the equilibrium is known. More precisely, the spatial distribution of iso-ψ surfaces on the (R, Z) plane is fixed. Additionally, we assume that the enclosed toroidal flux (6.22) is fixed, thereby fixing the spatial distribution of constant $\rho = \rho_{tor}$ surfaces $\rho_{tor}(R, Z)$. As a consequence, the geometric profile quantities G_1, G_2 and V', as well as J (6.56), (6.27)-(6.29) are fixed in time. Also, the flux-surface-averaged trapped-particle fraction, which enters in the bootstrap current and current drive efficiency (Section 6.4.2), is a function of the magnetic geometry; therefore, it is fixed as well. Finally, the vacuum toroidal magnetic field B_0 is assumed fixed. These restrictions mean that we are, in practice, (i) neglecting variations in diamagnetic effects which cause variations of $J(\rho)$, (ii) neglecting effects due to changes in the flux surface shapes such as motional electric fields and varying geometries, which are primarily the result of varying Shafranov shift as β evolves, and (iii) assuming a fixed plasma boundary in time.

Note that this is a weaker statement than assuming the Grad-Shafranov equilibrium to be fixed, indeed we do allow the poloidal flux profile $\psi(\rho)$, and hence q, j_{tor} etc to change in time. We merely fix the flux surface *geometry* and enclosed *toroidal flux*. By choosing a reference equilibrium, we can treat arbitrary plasma shapes as long as they are not time-varying. Analysis of several plasma equilibria, shown in Figure 7.1, indicates that unless the plasma β varies significantly with respect to the reference, the change in poloidal current density and Shafranov shift will be limited and acceptable. Even a doubling of β results in a variation of G_2/J and V' of less than 10%.

To alleviate this restriction it is also possible, though not implemented yet, to use a time-varying but pre-calculated parametrization for G_1, G_2, ... as a function of plasma
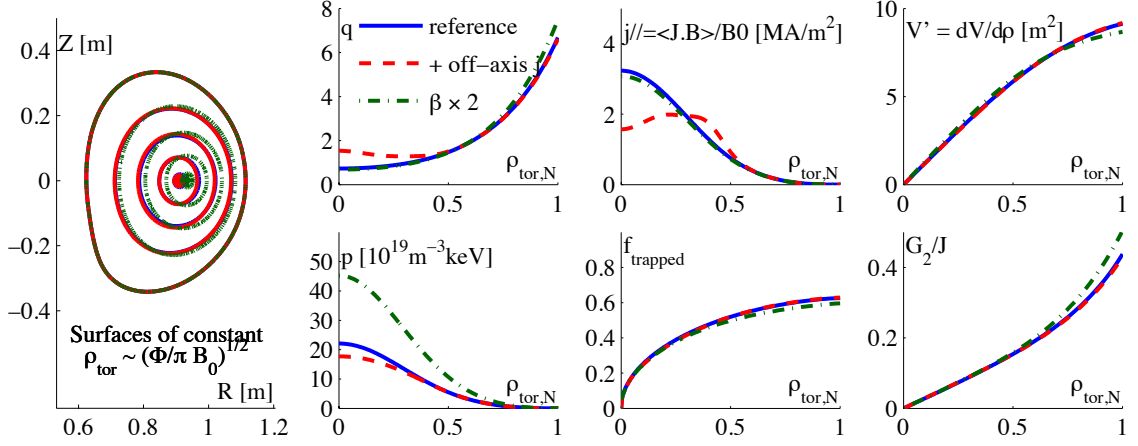
Figure 7.1: Set of three TCV equilibria illustrating the effect of assuming fixed flux surface geometry on the terms V', G_2/J appearing in (6.26). A reference equilibrium (blue, $-$) is perturbed by redistributing current density to give a reversed-shear q profile (red, $--$), and by doubling the pressure, i.e. β (green, $\cdot -$). The variation in V' and G_2/J can be seen to be within 10% of their reference value. Also the trapped particle fraction, which governs the neoclassical contribution to j_{bs}, $\sigma_\|$ and current drive efficiency, is hardly changed. The largest difference appears when changing the pressure through a change in Shafranov shift. The calculations were done using the fixed-boundary MHD equilibrium code CHEASE (Lutjens et al. 1996).

shape parameter such as elongation, Shafranov shift and triangularity. Alternatively, coupling to a Grad-Shafranov code can provide a consistent update of the magnetic equilibrium.

7.2.2 Parametrized heating and current drive sources

Common practice in transport physics codes is to recompute the power density and current density distribution at each simulation time step to reflect the changes due to the evolving plasma, using one of the codes mentioned in Section 6.4.2. These steps can often take a significant portion of the total computational time. In order to obtain a fast and lightweight code, the choice was made for RAPTOR to use only analytical parametrizations for heating and current drive sources. A simple but effective choice is to approximate power and current densities by weighted gaussian distributions which is the choice made for RAPTOR.

The power density to the electrons $P_{e,i}$ for the ith actuator is modeled as a Gaussian

$$P_{e,i}(\rho, t) = P_i(t) \exp\left\{ \frac{-4(\rho - \rho_{dep,i})^2}{w_{dep,i}^2} \right\} \Big/ \int_0^{\rho_e} \exp\left\{ \frac{-4(\rho - \rho_{dep,i})^2}{w_{dep,i}^2} \right\} V' \mathrm{d}\rho \quad (7.1)$$

with w_{dep} the deposition width and ρ_{dep} the location of the peak of the deposition. As for the current density, at this stage only ECCD is modeled. The current drive efficiency is known to be proportional to T_e/n_e (Prater 2004) and at the same time decrease with increased trapped particle fraction. This effect is modeled heuristically in the expression below.

$$j_{cd,i}(\rho, t) = c_{cd} e^{\rho^2/0.5^2} \frac{T_e}{n_e} e^{-4(\rho - \rho_{dep,i})^2/w_{cd,i}^2} P_i(t) \quad (7.2)$$

The factor c_{cd} is a machine-dependent proportionality factor (units A/m^5/eV/W) which can be chosen to scale the expression to experimentally obtained current drive values.

More complex parametrizations can be obtained by performing several runs of more complete codes for representative cases, parametrizing the resulting power and current densities based on the numerical results. It is worth noting that while the spatial distribution of EC and NBI deposition is relatively smooth and continuous with respect to plasma changes, LH and ICRF are much more sensitive to changes in the plasma and such parametrizations may prove to be more challenging.

7.2.3 Ad-hoc transport model and losses

RAPTOR, at present, solves only the energy transport equation for the T_e profile. To close the equations, expressions for the transport coefficients must be specified. A very simple model can be obtained by giving a closed-form expression for the heat diffusivity term χ_e (corresponding to $\chi_{T_e}^e$ in the notation of (6.55)) and setting all other coefficients to zero. In other words, the only driving term for electron heat flux is the electron temperature gradient, and convective transport is neglected. Though any analytical expression can be used, the model presently used in RAPTOR is a closed-form expression similar to that used in (Polevoi et al. 2002), (Albajar et al. 2005), (Garcia et al. 2010). It is constructed so as to reflect increasing confinement due to increasing I_p while having higher conductivity towards the plasma edge. A multiplicative term describes the confinement improvement due to low magnetic shear. The expression reads

$$\chi_e = \chi_{neo} + c_{ano}\rho q F(s) + \chi_{central} e^{-\rho^2/\delta_0^2} \tag{7.3}$$

where χ_{neo} is a (small) neoclassical diffusion term, chosen as a constant but which could be calculated from neoclassical physics. The anomalous diffusion is controlled by c_{ano}, and the presence of q in the anomalous diffusion term accounts for the lower transport at higher currents. $F(s)$ is a shear-dependent function to include the effect of improved confinement at low and negative magnetic shear, responsible for improved confiment (ic) scenarios (see Section 6.8):

$$F(s) = \frac{a_{ic}}{1 + \exp(w_{ic}(d_{ic} - s))} + (1 - a_{ic}) \tag{7.4}$$

here a_{ic}, w_{ic} and d_{ic} govern, respectively, the amount of confinement improvement, the sharpness of the transition and the value of the shear for which the transition takes place. The last term involving $\chi_{central}$ is an ad-hoc term representing a local confinement decrease at the center of the plasma, used to model the experimental observation that kinetic profiles are relatively flat near the center. It is consistent with sawtooth activity in the standard scenario and current hole effects in reverse shear scenarios (Fujita 2010). In this work we use $\delta_0 = 0.1$. An example of χ_e for a reversed-shear q profile is illustrated in Figure 7.2, showing the various terms of χ_e as well as $F(s)$ as a function of s.

Note that out of the seven transport model coefficients ($\chi_{neo}, c_{ano}, \chi_{central}, \delta_0, a_{ic}, w_{ic}, d_{ic}$), the first can in principle be obtained from neoclassical calculations, the final three only affect detailed behavior of enhanced confinement regimes, and $\chi_{central}, \delta_0$ have only a local effect on the central profile. The most important parameter in this model, having a global effect on confinement is the anomalous transport c_{ano}. This parameter was chosen
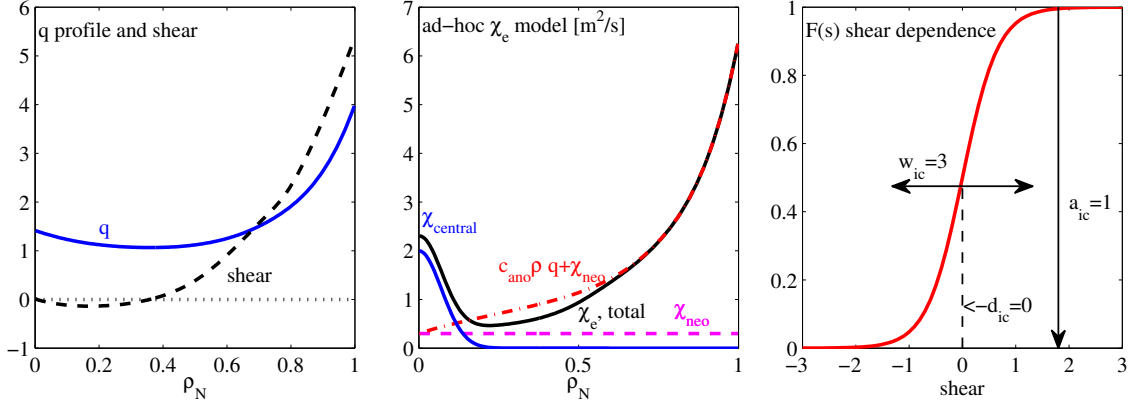
Figure 7.2: Illustration of ad-hoc electron transport model. Left panel: q and shear profile. Central panel: different components of Eq.(7.3), with and without shear enhancement factor F_s. Right panel: illustration of $F(s)$ vs s and dependence on parameters: d_{ic}, w_{ic} and a_{ic}.

by hand to yield reasonable profiles matching experimental observations, while no formal effort was made to quantitatively reproduce existing experiments. Note that c_{ano} could also be chosen to satisfy a confinement scaling such as the ITER scaling law (Doyle et al. 2007). H-mode pedestals are not modeled, thus the model can be used for L-mode only. Reduced transport at the edge can however easily be added by reducing the edge conductivity based on an analytical threshold for the transition.

As for direct loss terms for the electron energy appearing through P_e, sinks such as electron-ion equipartition losses, radiation losses and recombination have been neglected since the ion temperature evolution is not modeled.

7.2.4 Neoclassical conductivity and bootstrap current

The neoclassical conductivity and bootstrap current follow the equations given in (Sauter et al. 1999a), (Sauter et al. 2002b).

The neoclassical conductivity is factored as

$$\sigma_\parallel(\rho, t) = c_{neo}(\rho)\sigma_{Spitzer}(T_e(\rho, t)) \tag{7.5}$$

where the Spitzer conductivity is given by

$$\sigma_{Spitz} = \frac{1.9012 \cdot 10^4 T_e[eV]^{3/2}}{ZN(Z)\ln\Lambda_e}. \tag{7.6}$$

Here, $Z = Z_{eff}$ (6.59) is the effective charge and $N(Z) = 0.58 + 0.74/(0.76 + Z)$ depends weakly on Z (Sauter et al. 1999a). While Z_{eff} may in general vary spatially, it is chosen as a fixed quantity for the whole plasma, being difficult to diagnose accurately. The neoclassical correction c_{neo} depends on geometric effects as well as collisionality, but is, for now, evaluated only once for a given equilibrium and temperature profile. Variations in this neoclassical correction due to changes in collisionality (which are small) are therefore neglected in this model, although an extension would be straightforward as simple expressions for the collisionality as a function of T_e and n_e exist.

For the bootstrap current we use (6.30) which is rewritten, assuming $n_i = n_e$ and $\frac{\partial \ln T_i}{\partial \psi} = \frac{\partial \ln T_e}{\partial \psi}$ in a more convenient form involving derivatives of ρ.

$$j_{bs} = -\frac{2\pi J(\psi)R_0}{R_{pe}} \frac{\partial \rho}{\partial \psi} \left[\mathcal{L}_{31} \frac{\partial n_e}{\partial \rho} T_e + (\mathcal{L}_{31} + R_{pe}\mathcal{L}_{32} + (1 - R_{pe})\alpha \mathcal{L}_{34}) \frac{\partial T_e}{\partial \rho} n_e \right] \quad (7.7)$$

The assumption $\partial \ln T_i / \partial \psi = \partial \ln T_e / \partial \psi$ is appropriate because in cases where the T_e and T_i profiles have a very different shape (as is the case, for example, in electron transport barriers, or eITBs), the contribution of T_i to the bootstrap current is modest. One also has the option of assuming $\partial \ln n / \partial \psi = c_T \partial \ln T_e / \partial \psi$ with $c_T = 0.5$. This value is valid in transport barriers and has been shown to be due to the thermodiffusive pinch (Fable et al. 2006). Note that although this last assumption for the n_e contribution to the bootstrap current is inaccurate for non-eITB cases, the bootstrap contribution in such plasmas is in any case rather small. The coefficients α, $\mathcal{L}_{31}$, $\mathcal{L}_{32}$, $\mathcal{L}_{34}$ are functions of ρ which depend on collisionality and geometric effects which, as was the case for c_{neo}, above, are kept fixed in this work and calculated once with representative profiles and equilibrium. Note also that $\mathcal{L}_{34} \approx \mathcal{L}_{31}$, allowing further gains in execution speed if necessary.

7.2.5 Summary of equations

Under the approximations described above, Eq. (6.26) becomes

$$\sigma_{\parallel} \frac{\partial \psi}{\partial t} = \frac{R_0 J^2}{\mu_0 \rho} \frac{\partial}{\partial \rho} \left(\frac{G_2}{J} \frac{\partial \psi}{\partial \rho} \right) - \frac{V'}{2\pi \rho}(j_{bs} + j_{aux}) \quad (7.8)$$

And the electron transport equation, in the form of (6.53) becomes

$$V' \frac{\partial}{\partial t}[n_e T_e] = \frac{\partial}{\partial \rho} G_1 V' n_e \chi_e \frac{\partial T_e}{\partial \rho} + V' P_e \quad (7.9)$$

The equations can be written in a more general form as

$$m_\psi(T_e) \frac{\partial \psi}{\partial t} = \frac{\partial}{\partial \rho} \left(d_\psi \frac{\partial \psi}{\partial \rho} \right) + f_\psi(\psi, T_e) + \sum_{i=1}^m S_{i,\psi}(T_e) P_i(t) \quad (7.10)$$

$$m_{T_e} \frac{\partial T_e}{\partial t} = \frac{\partial}{\partial \rho} \left(d_{T_e}(\psi, T_e) \frac{\partial T_e}{\partial \rho} \right) + f_{T_e}(\psi, \frac{\partial \psi}{\partial t}) + \sum_{i=1}^m S_{i,T_e} P_i(t) \quad (7.11)$$

This is a set of two coupled, nonlinear parabolic PDEs on $\Omega = \{t \in \mathbb{R}, \rho \in \mathbb{R} \mid t_0 \le t \le t_f, \ 0 \le \rho \le \rho_e\}$. The boundary conditions are given by (6.31), (6.33) or (6.34) and by (6.63), (6.64).

The various terms read

$$m_\psi(T_e) = \frac{\sigma_{\parallel}(T_e)\mu_0 \rho}{J^2 R_0} \quad (7.12)$$

$$d_\psi = \frac{G_2}{J} \quad (7.13)$$

$$f_\psi(\psi, T_e) = \frac{V'}{2\pi \rho} j_{bs}(\psi, T_e) \quad (7.14)$$

$$m_{T_e} = V' n_e \quad (7.15)$$

$$d_{T_e}(\psi, T_e) = G_1 V' n_e \chi_e(\psi, T_e) \quad (7.16)$$

$$f_{T_e}(\psi, \dot{\psi}) = V' P_{OH}(\psi, \dot{\psi}) \quad (7.17)$$

and $S_{\psi,i}$, $S_{T_e,i}$ are, respectively, $V'/(2\pi\rho)$ times the time-independent part of Eq.(7.2) and V' times the time-independent part of Eq.(7.1). The time-dependent inputs $P_i(t)$ represent actuator powers. In this form, the same actuator can have both a heating and current drive effect as is often the case.

Having described the physics assumptions, we turn to the question of how to efficiently solve the equations numerically.

7.3 Spatial discretization

We treat the spatial discretization of the PDE in this section and the time integration for each simulation mode (interpretative or predictive) in the next two sections.

7.3.1 Finite elements

RAPTOR differs from most 1D transport codes in the choice for spatial discretization of the PDE. While most codes use finite difference schemes, RAPTOR uses finite elements. This method has the advantage of allowing a flexible choice of basis functions, a natural implementation of a non-equidistant mesh as well as reduction of the order of spatial derivatives required through integration by parts. The infinite-dimensional PDEs (7.10) - (7.11) for the continuous functions $\psi(\rho, t)$, $T_e(\rho, t)$ are transformed into a set of finite-dimensional ODEs in the finite element coefficients by writing:

$$\psi(\rho, t) = \sum_{\alpha=1}^{n_{sp}} \Lambda_\alpha(\rho)\hat{\psi}_\alpha(t) \quad \text{and} \quad T_e(\rho, t) = \sum_{\alpha=1}^{n_{sp}} \Lambda_\alpha(\rho)\hat{T}_{e\alpha}(t) \tag{7.18}$$

where as finite element basis functions $\Lambda_\alpha(\rho)$ we choose non-periodic B-splines (de Boor 2001) having finite support, defined using a set of *knots*

$$\rho_j \in [\rho_1, \ldots, \rho_{n_{kts}}] \tag{7.19}$$

with $0 = \rho_1 < \rho_2 < \ldots < \rho_{n_{kts}} = \rho_e$.

One has the option of choosing splines of arbitrary order, but in this work cubic splines were chosen as this guarantees continuity up to the second derivative, ensuring continuity of, for example, current densities and magnetic shear. The set of basis functions is furthermore chosen such that all elements have zero derivative at $\rho = 0$. This ensures that the solutions automatically satisfy the Neumann boundary conditions (6.31) and (6.63).

Figure 7.3 shows an example of a $\psi(\rho)$ profile approximated as a sum of cubic splines (Fig.7.3a) on a non-equidistant set of 16 knots. Also shown are the q profile and j_{tor} profile computed directly from the spline representation of $\psi(\rho)$. One can clearly observe that j_{tor}, which is a function of the second derivative of ψ, is continuous but not differentiable if we choose third order splines. Note also that with this choice of splines the edge values are determined only by the first and last spline coefficients.

With this approximation, the PDEs (7.10), (7.11) are rewritten into ODEs: substituting (7.18) into (7.10) and (7.11), then projecting both equations onto a set of basis functions $\Lambda_\beta(\rho)$, and integrating by parts, the PDEs are recast into two matrix-vector
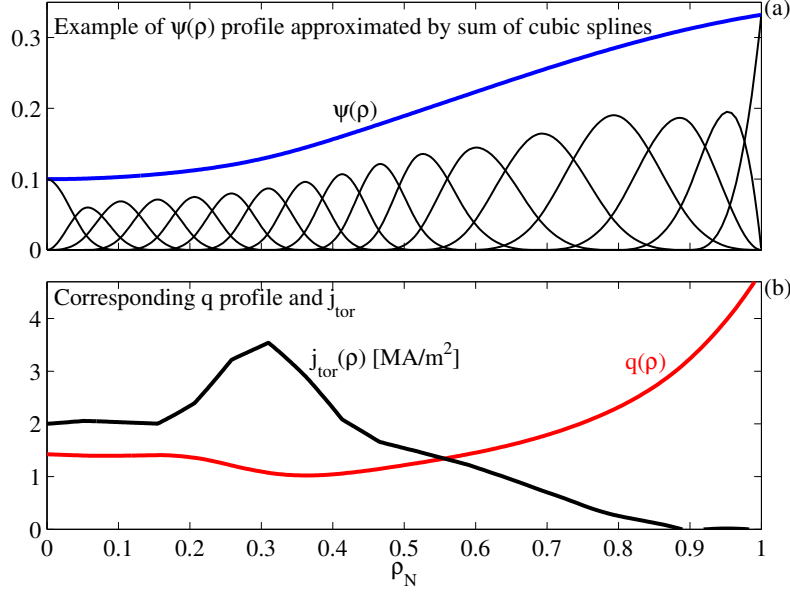
Figure 7.3: Illustration of an example $\psi(\rho)$ profile expressed as the sum of 18 non-periodic cubic splines defined by choosing a set of 16 non-equidistant knot points on the ρ grid. Fig.7.3a shows individual weighted splines and the resulting ψ profile following Eq.(7.18). Fig.7.3b shows corresponding q profile (6.37) and j_{tor} profile (6.36). Note that since $j_{tor} \sim \partial^2 \psi/\partial\rho^2$, j_{tor} is continuous but not differentiable at the knot points with this choice of basis functions.

equations involving $\hat{\boldsymbol{\psi}} = [\hat{\psi}_1, \ldots, \hat{\psi}_{n_{sp}}]^T$ and $\hat{\mathbf{T}}_e = [\hat{T}_{e1}, \ldots, \hat{T}_{en_{sp}}]^T$.

$$F = \mathbf{0} \quad = -\mathbf{M}_\psi(\hat{\mathbf{T}}_\mathbf{e})\dot{\hat{\boldsymbol{\psi}}} - \mathbf{D}_\psi\hat{\boldsymbol{\psi}} + \mathbf{B}_\psi(\hat{\mathbf{T}}_\mathbf{e})\mathbf{u} + \mathbf{f}_\psi(\hat{\boldsymbol{\psi}}, \hat{\mathbf{T}}_e) \quad (\psi \text{ evolution}) \qquad (7.20)$$

$$G = \mathbf{0} \quad = -\mathbf{M}_{T_e}\dot{\hat{\mathbf{T}}}_e - \mathbf{D}_{T_e}(\hat{\boldsymbol{\psi}}, \hat{\mathbf{T}}_\mathbf{e})\hat{\mathbf{T}}_e + \mathbf{B}_{T_e}\mathbf{u} + \mathbf{f}_{T_e}(\hat{\boldsymbol{\psi}}, \dot{\hat{\boldsymbol{\psi}}}) \quad (T_e \text{ evolution}) \qquad (7.21)$$

Where $\hat{\boldsymbol{\psi}}, \hat{\mathbf{T}}_e \in \mathbb{R}^{n_{sp}}$. Matrices $\mathbf{M}_\psi, \mathbf{D}_\psi, \mathbf{M}_{T_e}, \mathbf{D}_{T_e} \in \mathbb{R}^{n_{sp} \times n_{sp}}$; $\mathbf{B}_\psi, \mathbf{B}_{T_e} \in \mathbb{R}^{n_{sp} \times m+1}$ and vectors $\mathbf{f}_\psi$ and $\mathbf{f}_{T_e}$ have elements defined by equations (D.12) - (D.19). Note that $\mathbf{M}$ and $\mathbf{D}$ are sparse and have a band structure with bandwidth $2d + 1$ where d is the order of the chosen splines. Details on how the terms in the matrices are efficiently calculated are given in Appendix D.1.3. The input vector $\mathbf{u}$ depends on the choice of boundary condition for the flux diffusion equation:

$$\mathbf{u}(t) = \begin{cases} [P_1(t), \ldots, P_m(t), \Psi_{OH}(t)]^T & \text{if Eq.(6.33) is used} \\ [P_1(t), \ldots, P_m(t), I_p(t)]^T & \text{if Eq.(6.34) is used} \end{cases} \qquad (7.22)$$

In equations (7.20) and (7.21), the $\mathbf{M}$ matrices represent *mass* matrices; the $\mathbf{D}$ matrices are *stiffness* terms and the $\mathbf{B}$ matrices are *input* matrices, translating how the influence of the input vector gets distributed over the profiles. Finally the $\mathbf{f}$ terms are endogenous forcing terms, or sources, which are caused by the profiles themselves.

Using these definitions, the boundary conditions now appear explicitly either as terms in the input vector (7.22) or in the forcing function $\mathbf{f}_{T_e}$ (D.19). Since we choose $T_{e,edge}$ to be a fixed prescribed value throughout this work, we do not include it in the input vector.

Having discussed the main equations and assumptions of the RAPTOR code, we now turn to the different modes of operation.

7.3.2 Computing quantities related to the profile state

It is important to realize that using finite elements we can calculate any related quantity, including all those listed in Sections 6.4.4 and 6.5.5 at any time t and location ρ, including spatial derivatives, directly from the spline coefficient vectors $\hat{\boldsymbol{\psi}}$, $\hat{\mathbf{T}}_e$.

In particular, quantities which could be obtained by applying linear (differential) operators to the ψ or T_e profile, can now be obtained at an arbitrary ρ by taking the inner product of the coefficient vector with another vector[1]. To provide a few examples:

$$\iota(\rho, t) \quad \approx \mathbf{c}_\iota^T(\rho)\hat{\boldsymbol{\psi}}(t), \tag{7.23}$$

$$j_{tor}(\rho, t) \quad \approx \mathbf{c}_{j_{tor}}^T(\rho)\hat{\boldsymbol{\psi}}(t), \tag{7.24}$$

$$U_{pl}(\rho, t) \quad \approx \mathbf{c}_\Lambda^T(\rho)\dot{\hat{\boldsymbol{\psi}}}(t), \tag{7.25}$$

$$T_e(\rho, t) \quad \approx \mathbf{c}_\Lambda^T(\rho)\hat{\mathbf{T}}_e(t), \tag{7.26}$$

$$\frac{\partial U_{pl}}{\partial \rho}(\rho, t) \quad \approx \mathbf{c}_{\Lambda'}^T(\rho)\dot{\hat{\boldsymbol{\psi}}}(t), \tag{7.27}$$

$$\frac{\partial T_e}{\partial \rho}(\rho, t) \quad \approx \mathbf{c}_{\Lambda'}^T(\rho)\hat{\mathbf{T}}_e(t), \tag{7.28}$$

where the vector elements are given by

$$[\mathbf{c}_\iota(\rho))]_\alpha = \frac{1}{2\pi B_0 \rho}\frac{\partial \Lambda_\alpha}{\partial \rho}, \tag{7.29}$$

$$[\mathbf{c}_{j_{tor}}(\rho)]_\alpha = \frac{2\pi R_0}{\mu_0 V'}\left(\frac{\partial G_2}{\partial \rho}\frac{\partial \Lambda_\alpha}{\partial \rho} + G_2\frac{\partial^2 \Lambda_\alpha}{\partial \rho^2}\right), \tag{7.30}$$

$$[\mathbf{c}_\Lambda^T(\rho)]_\alpha = \Lambda_\alpha, \tag{7.31}$$

and

$$[\mathbf{c}_{\Lambda'}^T(\rho)]_\alpha = \frac{\partial \Lambda_\alpha}{\partial \rho}. \tag{7.32}$$

7.4 Interpretative mode

RAPTOR can be run in interpretative mode, in which only the poloidal flux equation (7.20) is solved. The evolution of $T_e(\rho, t)$, as well as all other kinetic profiles required to compute the $\sigma_\parallel$, j_{bs} and j_{aux} are assumed to be known, usually from experimental data. This section describes the numerical scheme for the time integration in this mode.

7.4.1 Time discretization

To discretize the continuous-time equation (7.20), a time grid $t = [t_0, \ldots, t_k, \ldots, t_M]$ is chosen. After combining the source terms $\mathbf{s}_\psi = \mathbf{B}_\psi(\hat{\mathbf{T}}_e)\mathbf{u} + \mathbf{f}_\psi(\hat{\boldsymbol{\psi}}, \hat{\mathbf{T}}_e)$ one can write a general Crank-Nicholson-type discretization scheme

$$\mathbf{M}_\psi(t_{k+\frac{1}{2}})\left(\frac{\hat{\boldsymbol{\psi}}_{k+1} - \hat{\boldsymbol{\psi}}_k}{\Delta t}\right) = -\mathbf{D}_\psi(t_{k+\frac{1}{2}})\left(\theta\hat{\boldsymbol{\psi}}_{k+1} + (1-\theta)\hat{\boldsymbol{\psi}}_k\right) + \mathbf{s}_\psi(t_{k+\frac{1}{2}}) \tag{7.33}$$

---

[1]More formally, we can obtain the projection of these profiles on the space $\mathcal{V}_h$ spanned by the finite-element basis functions or their derivatives.

which is second-order accurate. For practical reasons, let us approximate the terms above in order to obtain the most stable numerical scheme requiring no iterations, at the expense of being less accurate. This is achieved by choosing

$$\mathbf{M}_\psi(t_{k+\frac{1}{2}}) \approx \mathbf{M}_\psi(t_k) = \mathbf{M}_{\psi,k}, \tag{7.34}$$

$$\mathbf{s}_\psi(t_{k+\frac{1}{2}}) \approx \mathbf{s}_\psi(t_k) = \mathbf{s}_{\psi,k}, \tag{7.35}$$

$$\mathbf{D}_\psi(t_{k+\frac{1}{2}}) = \mathbf{D}_\psi(t_k) = \mathbf{D}_\psi \quad \text{(time-independent)}, \tag{7.36}$$

$$\theta = 1. \tag{7.37}$$

This gives the following difference equation, implicit in time:

$$(\mathbf{M}_{\psi,k} + \Delta t \mathbf{D}_\psi)\hat{\psi}_{k+1} = (\mathbf{M}_{\psi,k})\hat{\psi}_k + \Delta t \mathbf{s}_{\psi,k} \tag{7.38}$$

This linear system is to be solved for each time step yielding an update $\hat{\psi}_{k+1}$. Note that the elements $\mathbf{M}_{\psi,k}$ and $\mathbf{s}_{\psi,k}$ of this linear system are all calculated based on the current time step, k, avoiding the need to iterate: a step forward in time to step $k+1$ is made based only on information available at time step k. Experience suggests that when the time step is taken sufficiently small with respect to the characteristic time scales of the equations, errors introduced by the approximations (7.34)-(7.37) are acceptably small. Each time step requires the solution of the linear system(7.38), the left-hand side of which contains a banded, positive definite, symmetric matrix such that the problem can be efficiently solved by LDL^T (Cholesky) decomposition (Golub et al. 1996).

7.4.2 Benchmarking vs ASTRA

To validate and benchmark the Intepretative-RAPTOR algorithm, we can compare simulation results to results from the ASTRA code. The results are shown in Figure 7.4.

Input data was chosen so as to provide a dynamically varying set of profiles. The total plasma current was prescribed as a triangular waveform varying from 100kA to 200kA as shown in Fig.7.4a. Additionally, a set of artificial T_e, n_e, T_i, n_i profiles were generated, all of which had a Gaussian shape and the temperature profiles were programmed to evolve in time following a square wave signal between 0.5 and 1.5keV as shown in Fig.7.4b. This data was then fed to Interpretative-RAPTOR, run using a given baseline plasma equilibrium. The same data was fed to ASTRA, using a parametrized shape for the LCFS based on the elongation, triangularity and minor radius of the baseline equilibrium. Recall that for ASTRA only the LCFS parameters are specified but the internal equilibrium is solved self-consistently, while for RAPTOR the entire equilibrium is static. Z_{eff} was set to 3.5 for both cases. The simulations were run for sufficient time for transient effects due to initial conditions to subside, and a final period of the simulation is compared.

One can observe an excellent agreement between all displayed quantities. Variations were found to be due to the different treatment of the equilibrium due to the fixed equilibrium assumption in RAPTOR. Nevertheless, remarkably good agreement is found in critical quantities such as q profile locations, which are virtually indistinguishable, even with large variations of T_e, and therefore β, by a factor 3.
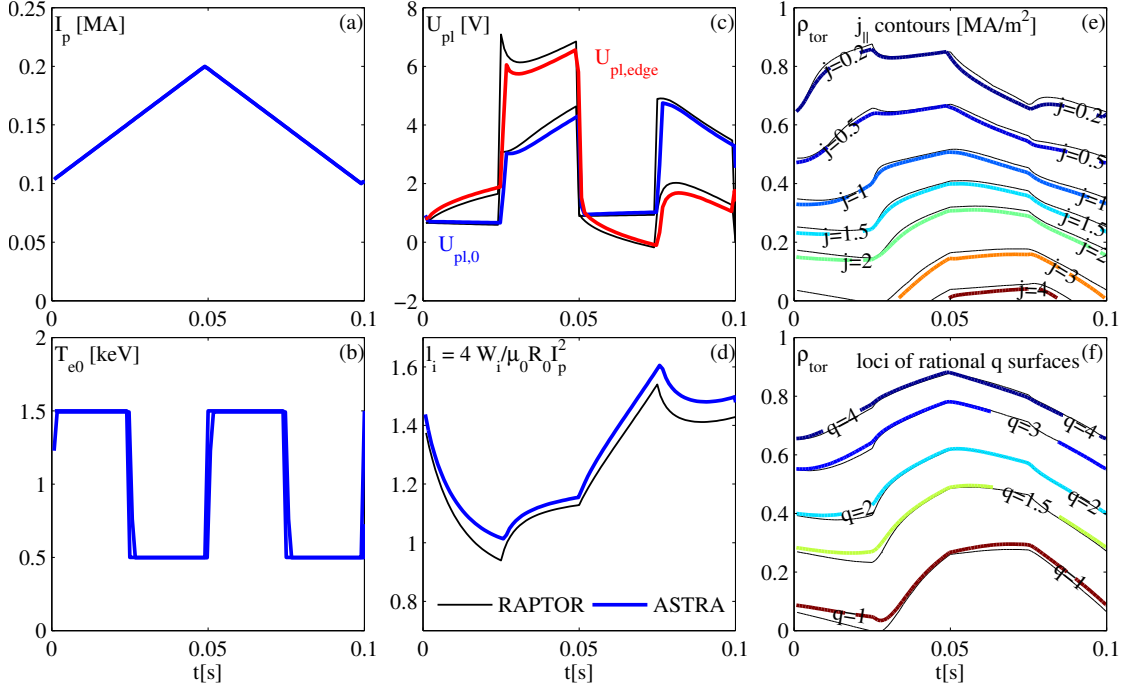
Figure 7.4: Benchmark simulations comparing RAPTOR and ASTRA results for artificial input profiles. A set of Gaussian temperature and density profiles were specified, which were scaled in time to a square-wave shaped central temperature time trace shown in (b). The colored traces represent ASTRA results and the black lines are the corresponding result from RAPTOR. One can see a very good match for the central and edge loop voltage (c), the internal inductance (d) and contour lines of $j_\parallel$ (e) and q surface locations (f).

7.5 Predictive-RAPTOR

The predictive version of the RAPTOR code solves the coupled system (7.20), (7.21). The numerical scheme is different, owing to the stiff and strongly nonlinear nature of the equations. A fully implicit scheme is used as summarized below. Uniquely, the predictive-RAPTOR code returns not only the time evolution of ψ and T_e, but also sensitivities of the solution to a given set of parameters. This is discussed in some depth in Section 7.5.2.

7.5.1 Algorithm

For notational simplicity, equations (7.20)-(7.21) are recast in compact form by defining the state

$$x(t) = \left[\begin{array}{c} \hat{\boldsymbol{\psi}}(t) \\ \hat{\mathbf{T}}_{\mathbf{e}}(t) \end{array} \right] \tag{7.39}$$

and combining both equations into

$$f = \left[\begin{array}{c} F(\dot{x}, x, u) \\ G(\dot{x}, x, u) \end{array} \right] \tag{7.40}$$

thus obtaining

$$f(\dot{x}(t), x(t), u(t)) = 0 \; \forall \; t \tag{7.41}$$

Here the bold notation for vectors and matrices has been dropped.

After defining a time grid $t = [t_0, \ldots, t_k, \ldots, t_M]$, the continuous-time equations (7.20)-(7.21) are discretized in time by choosing

$$\dot{x}(t_k) = (x_{k+1} - x_k)/\Delta t, \tag{7.42}$$

$$x(t_k) = \theta x_{k+1} + (1 - \theta) x_k, \tag{7.43}$$

and

$$u(t_k) = u_k. \tag{7.44}$$

We can then rewrite the discrete-time equivalent of (7.41)

$$\tilde{f}_k \equiv \tilde{f}(x_{k+1}, x_k, u_k) = 0 \quad \forall\, k \tag{7.45}$$

Varying θ between $\theta = 1$ and $\theta = 0$ allows one to vary between a fully implicit and fully explicit method. We choose a fully implicit method $\theta = 1$, which has advantages for such a stiff system since the time step can be taken quite large without risking numerical stability problems[2].

A disadvantage is that the nonlinear equation (7.45) must be solved iteratively. This is done by a series of Newton-Raphson iterations at each time step: with given x_k from the previous time step, and known u_k, a solution x_{k+1} to the nonlinear equation (7.45) is found. Details of how the Newton iterations are implemented, as well as a summary of the algorithm, are given in D.3.1. It is important to note that in the Newton step the Jacobian matrix $\mathcal{J}_{k+1}^k = \partial \tilde{f}_k / \partial x_{k+1}$ is computed and factored, and that this matrix will be important in calculating the state sensitivities as explained in the following section.

7.5.2 Trajectory sensitivity

When simulating the system of equations (7.10)-(7.11), it will be important to evaluate not only the evolution of the state x in time, but also the sensitivity of its evolution to a set of parameters. This information will turn out to be very useful for purposes described in Section 9.2, but in this section we will already describe how these sensitivities are computed numerically.

The definition of "parameters" is kept purposely general at this stage, but we may restrict ourselves to model parameters (for example one of the transport parameters appearing in (7.3)) or input parameters (affecting the temporal evolution of the actuator trajectories or initial conditions). It is important to distinguish between the model states (for example ψ) and model outputs (for example j_{tor}) on one hand, and parameters on the other. Parameters affect the time evolution of the simulation and are not a simulation result.

The sensitivity of the state evolution to a set of parameters can be computed using the so-called Forward Sensitivity Analysis method (Cacuci 1981). Differentiating (7.45)

---

[2]A similar choice is documented for the BALDUR code (Singer et al. 1988) which solves structurally identical equations. However, note that BALDUR uses the more conventional predictor-corrector method rather than full Newton steps

with respect to a vector of parameters $p \in \mathbb{R}^{n_p}$ we obtain the *forward sensitivity equation* with respect to p:

$$0 = \frac{\mathrm{d}\tilde{f}_k}{\mathrm{d}p} = \frac{\partial \tilde{f}_k}{\partial x_{k+1}} \frac{\partial x_{k+1}}{\partial p} + \frac{\partial \tilde{f}_k}{\partial x_k} \frac{\partial x_k}{\partial p} + \frac{\partial \tilde{f}_k}{\partial u_k} \frac{\partial u_k}{\partial p} + \frac{\partial \tilde{f}_k}{\partial p} \tag{7.46}$$

This linear matrix equation is recursively solved starting from the initial condition $\frac{\partial x_0}{\partial p}$, yielding $\frac{\partial x_{k+1}}{\partial p}$, for $k \in [1, \ldots, M]$. We will now treat each of the terms in slightly more detail.

- The first term on the r.h.s. contains the Jacobian $\mathcal{J}_{k+1}^k = \frac{\partial \tilde{f}}{\partial x_{k+1}}$, which has already been computed and factored in the Newton step (D.34), the solution of (7.45).

- The second term contains the Jacobian $\mathcal{J}_k^k = \frac{\partial \tilde{f}}{\partial x_k}$, which has to be computed. However the expressions for the terms in this matrix have the same structure as those of $\mathcal{J}_{k+1}^k$, and can be obtained by substituting $\Delta t \rightarrow -\Delta t$ and $\theta \rightarrow (1 - \theta)$ in (D.29)-(D.33). This additional matrix can therefore be additionally computed with minimal effort. Note that there is no need to factor the matrix.

- The third term on the r.h.s. is nonzero only for input parameters, which affect the model evolution via the input trajectories, having nonzero $\frac{\partial u_k}{\partial p}$ for some k. Note that $\frac{\partial \tilde{f}_k}{\partial u_k}$ is related to the **B** matrices in (7.20)-(7.21).

- The last term on the r.h.s., on the other hand, is nonzero only for model parameters, i.e. parameters which affect the model directly by altering the equations. Depending on the parameter considered, the appropriate form for $\frac{\partial \tilde{f}_k}{\partial p}$ can be derived analytically.

To compute the state sensitivities with this method one needs to evolve one ODE of the form (7.46) for each parameter in the parameter vector p. The additional computational burden for performing this calculation at the same time as evolving the main PDE is modest, as long as the number of parameters is not excessively large. Indeed, one has to be careful in correctly computing the various derivatives, but since the Jacobians are already known from the Newton iterations, this important step does not need to be repeated. In the following section we will provide a practical example of the information which can be obtained from the state sensitivities.

7.5.3 A simulation example

We now provide a simulation example to illustrate a typical run of Predictive-RAPTOR, for benchmarking as well as to point out some salient features. It will also serve as an example to demonstrate the usefulness of the state sensitivities. This example also serves as an introduction to the operationally relevant plasma current ramp-up scenarios which will be studied more in-depth in later chapters.

Simulation parameters

For this simulation and for all those presented in this thesis, unless specified otherwise, we use the same fixed 2D background equilibrium from an existing TCV shot with elongation

$\kappa = 1.4$ and triangularity $\delta = 0.3$. The other parameters of the simulation, including transport model parameters, are those listed in Table 7.1.

Table 7.1: Simulation parameters. See Eq.(7.3) for the meaning of the transport coefficients.

Parameter	Value
Equilibrium	TCV#41083@1.0s
B_0	1.44T
R_0	0.88m
Z_{eff}	3.5
χ_{neo}	$0.5\mathrm{m}^2\mathrm{s}^{-1}$
c_{ano}	$7.0\mathrm{m}^2\mathrm{s}^{-1}$
a_{ic}	1.0
w_{ic}	3.0
d_{ic}	0.0
$\chi_{central}$	$10.0\mathrm{m}^2\mathrm{s}$
δ_0	0.15

For this first example, we choose $\Delta t = 0.5$ms and $n_{kts} = 41$. These temporal and spatial grids are chosen to be overly dense at this stage: a more thorough investigation of the appropriate gridsize is carried out using a set of benchmarks presented in Appendix D.3.2.

Benchmarking vs ASTRA

To validate the implementation, a benchmark simulation is shown comparing the output of Predictive-RAPTOR to that of ASTRA. First, a simulation was run in Predictive-RAPTOR with the I_p and P_{aux} trajectories shown in Figure 7.5a. Then, the same I_p and P_{aux}, j_{aux} and plasma shape parameters were used in an ASTRA simulation, in which the transport model (7.3) has also been implemented. Again, in both cases, the input trajectory sequence was repeated several times to get rid of effects of initial conditions. The equations solved by ASTRA are identical to those in Predictive-RAPTOR except that ASTRA updates the internal Grad-Shafranov equilibrium and flux surface shapes while RAPTOR does not. Still, as shown in Figure 7.5, the results compare very well, except for some discrepancy at the center which is attributed to the changing flux surfaces. This, however, does not have a strong effect on the q profile evolution, which is the key parameter to be simulated.

Example of plasma trajectory evolution during ramp-up

Next, we simulate a current ramp-up from 80kA ($q_{95} \approx 13$) to 200kA ($q_{95} = 4.8$) in 25ms, followed by another 25ms period of flat I_p and a step of 1MW of EC power deposited at $\rho = 0.4$ ($w_{dep} = 0.35$), giving both a heating and current drive effect. These actuator input trajectories are plotted against time in Fig.7.6a. The remaining panels of Figure 7.6 show a collection of simulation outputs. Fig.7.6b shows contour plots of the rotational transform $\iota(\rho, t)$ in space (vertical axis) and time (horizontal axis), with superimposed contours showing the location of rational q surfaces. Similarly, Fig.7.6c and Fig.7.6d show
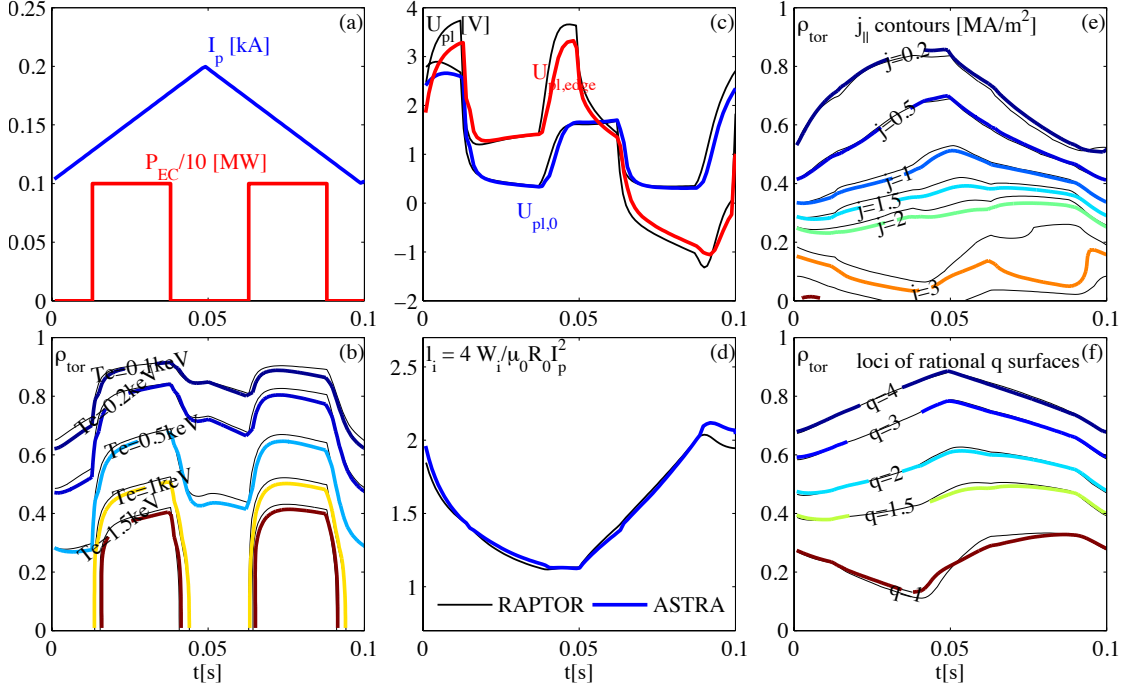
Figure 7.5: Benchmarking of Predictive-RAPTOR (black, thin) vs. ASTRA (color, thick), run with the same transport model and current drive profile. This confirms that the 1-D model used in Predictive-RAPTOR can reproduce the results of the 1.5D profile+equilibrium simulation from ASTRA.

the contours of electron temperature T_e and plasma loop voltage profile U_{pl}, respectively. The four rightmost panels show a collection of profiles at the final time of the simulation ($t = 50$ms). Fig.7.6e shows the current density profile, separated into Ohmic, auxiliary and bootstrap components. Fig.7.6f shows the safety factor profile and shear, Fig.7.6g shows the kinetic profiles T_e and n_e, as well as the loop voltage profile U_{pl}. Finally Fig.7.6h shows the power sources, separated into Ohmic and auxiliary power, as well as the thermal diffusivity profile χ_e.

Now let us examine some of the main features which are visible on these plots

- In the period before the auxiliary power switch-on, the q surfaces move in response to the diffusion of current in the plasma and the q profile drops slightly below 1 in the center. As the plasma is relatively cold ($T_e < 1$keV) the loop voltage is also relatively high and is higher at the edge of the plasma: the edge loop voltage, induced by the ohmic transformer, is effectively pulling the I_p ramp of plasma current at this stage.

- At $t = 25$ms, when 1MW of auxiliary power is added, the electron temperature can be seen in Fig.7.6c to rapidly increase on a confinement time scale of a few ms. There is also an effect on the q profile evolution, as witnessed by the discontinuity in the rational q surface evolution. The decreased resistivity causes a reduction in the overall loop voltage and, combined with auxiliary current drive, causes the current distribution to change with respect to the Ohmic profile. We can also witness

the lower loop voltage around $\rho = 0.3$ for $t > 25$ms caused by the back-EMF (electromotive force) in reaction to the auxiliary current drive.

- The profiles at the final time $t = 50$ms, shown in the rightmost panels, feature a centrally flat q profile with $|s| < 0.5$ for $\rho < 0.46$. This state resembles that of the "hybrid" plasma scenario in terms of q profile, albeit with lower β and thus lower bootstrap current fraction (cf. Section 6.8), and excluding the important H-mode pedestal. However, examining the U_{pl} profile in Fig.7.6g shows that the profiles have yet to reach a stationary state. The central Ohmic current would peak further and the central q would drop if the simulation were allowed to continue beyond this time. Also, notice that the Ohmic power constitutes a small fraction of the total input power, the bulk of which comes from the auxiliary heating source. The thermal diffusivity profile, also shown in Fig.7.6h, is low in the region of low shear $\rho \sim 0.3$ but increases again due to the peaked central heat conductivity introduced, as explained in Section 7.2, to obtain a flat central T_e profile.

Illustration of state sensitivities

The example presented above also provides an opportunity to illustrate the concept of state sensitivities introduced in Section 7.5.2. In the present example we choose to define p precisely as the level of auxiliary power to be injected at $t = 25$ms. Therefore, $p = p_0 = 1$MW. This specific choice to parametrize the actuator inputs in time with a discrete parameter can be seen as a special case of *control vector parametrization*, a concept which will be generalized in Section 9.2.1.

At this point, we will simply examine the information given by the state sensitivity to this parameter $\partial x/\partial p$, which is an output of the Predictive-RAPTOR simulation. Recalling the definition of x (7.39) and the profile quantities which can be derived from x such as (7.23)-(7.28), we actually have knowledge of the sensitivities $\partial \iota(\rho,t)/\partial p$, $\partial j_\parallel/\partial p$, $\partial T_e/\partial p$ etc. From this information, we can approximate, to first order, the perturbed evolution of the profiles due to a perturbation δp with respect to p_0, for example

$$\iota(\rho,t)|_{p=p_0+\delta p} \approx \iota(\rho,t)_{p=p_0} + \frac{\partial \iota(\rho,t)}{\partial p}\delta p \tag{7.47}$$

Following this method, we compute the perturbed evolution of the various profiles for $\delta p = \pm 200$kW, shown in Figure 7.7. In these figures, the gray curves show the reference, unperturbed case $p_0 = 1$MW, identical to those shown in Figure 7.6. The blue and red curves show the profiles for $\delta p = +0.2$MW and $\delta p = -0.2$MW (Fig.7.7a), respectively. As one can see from Figure 7.7b-d, the profile evolutions are identical for $t < 25$ms. After this time, the additional or reduced auxiliary power causes a different evolution of the profiles.

Qualitatively, we notice that lower power (red) causes more peaked current density profile (Fig.7.7e), lower q profile in the center and higher shear (Fig.7.7f), lower T_e profile and higher loop voltage due to the increased plasma resistivity (Fig.7.7g). Conversely, more power (blue) causes a more reversed q profile with lower (negative) shear (Fig.7.7g), higher T_e and reduced loop voltage.

The computed variation in the profiles is, as mentioned, a linearization with respect to the original (unperturbed) profile evolution. We therefore also compare the perturbed
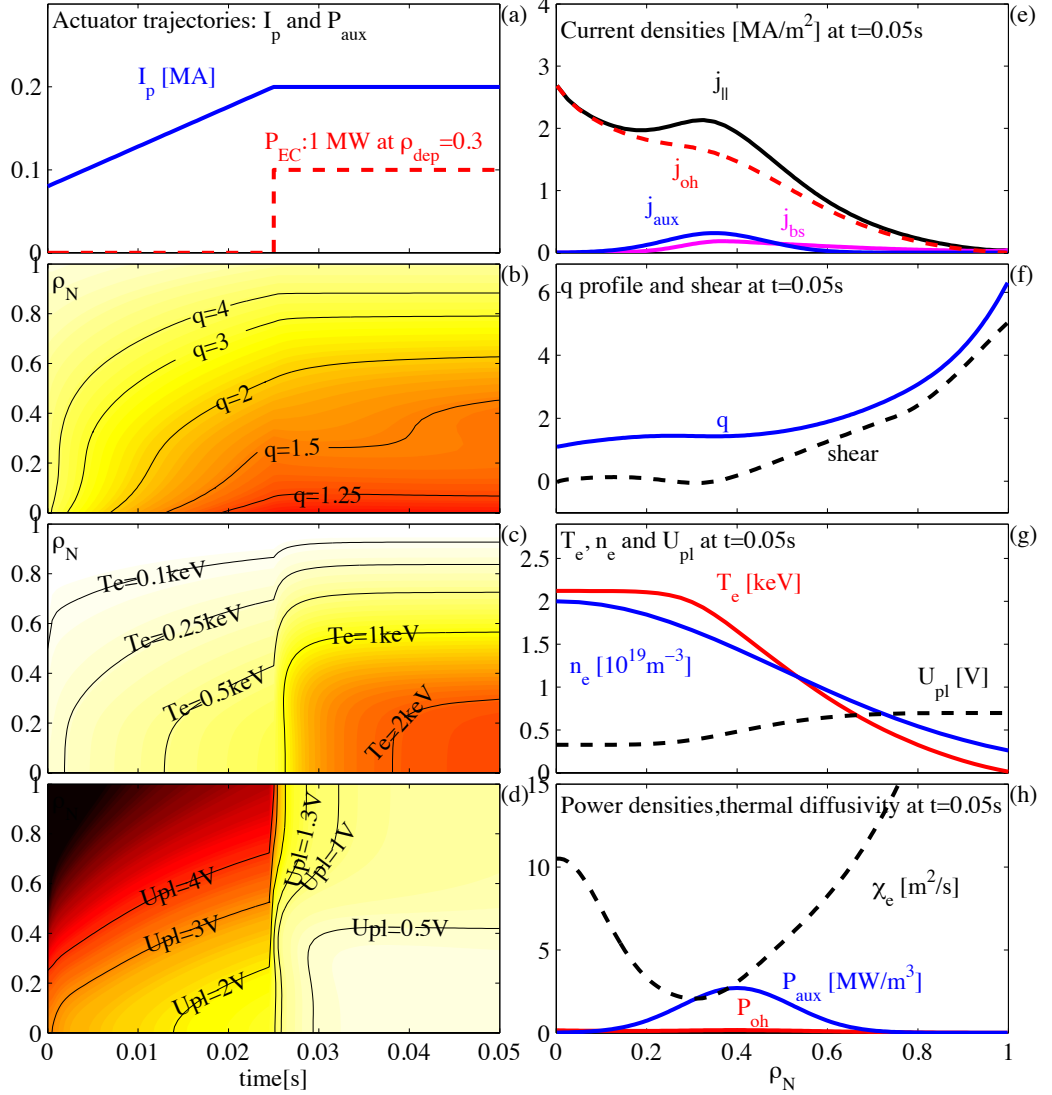
Figure 7.6: Example of tokamak plasma profile evolution during current ramp-up followed by auxiliary current drive switch-on (a), simulated using Predictive-RAPTOR. The temporal evolution of q, T_e and loop voltage U_{pl} profiles shown in space and time in (b),(c),(d), respectively, illustrates how the off-axis current drive creates a q profile slightly above 1 and results in increased plasma temperature and reduced plasma loop voltage. Various profiles at the end of the simulation period $t = 50$ms are shown in (e),(f),(g),(h). It is observed that the bootstrap current plays a minor role in this plasma, and that the off-axis current results in a magnetic shear close to 0 in the region $\rho < 0.4$.

T_e profile evolution computed with this method to the result obtained from a (new) full nonlinear simulation, i.e. running a new Predictive-RAPTOR simulation again for $p_0 = 1.2$MW. The difference between the two T_e profiles obtained in this way is shown in Fig.7.7h, showing a maximum error of 5eV, which is remarkably small when compared to the typical central T_e values of ~ 2keV. Considering that δp is, in our example, 20% of p_0, one can expect the local linearization to be even more exact for smaller perturbations.

It is important to realize that variation of this single (scalar) parameter impacts the

global evolution of the profiles in space and time, and that the differential variation in every plasma quantity at any point in space and time can be obtained, to first order, by simple operations from the sensitivities $\partial x/\partial p$, which in turn have been previously obtained at low computational cost, in parallel with the original simulation. In essence, $\partial x/\partial p$ is the gradient of the profile evolution trajectories with respect to p. The knowledge of these gradients will prove to be of crucial importance in later sections when we attempt to find a numerical optimum in a multi-dimensional parameter space.
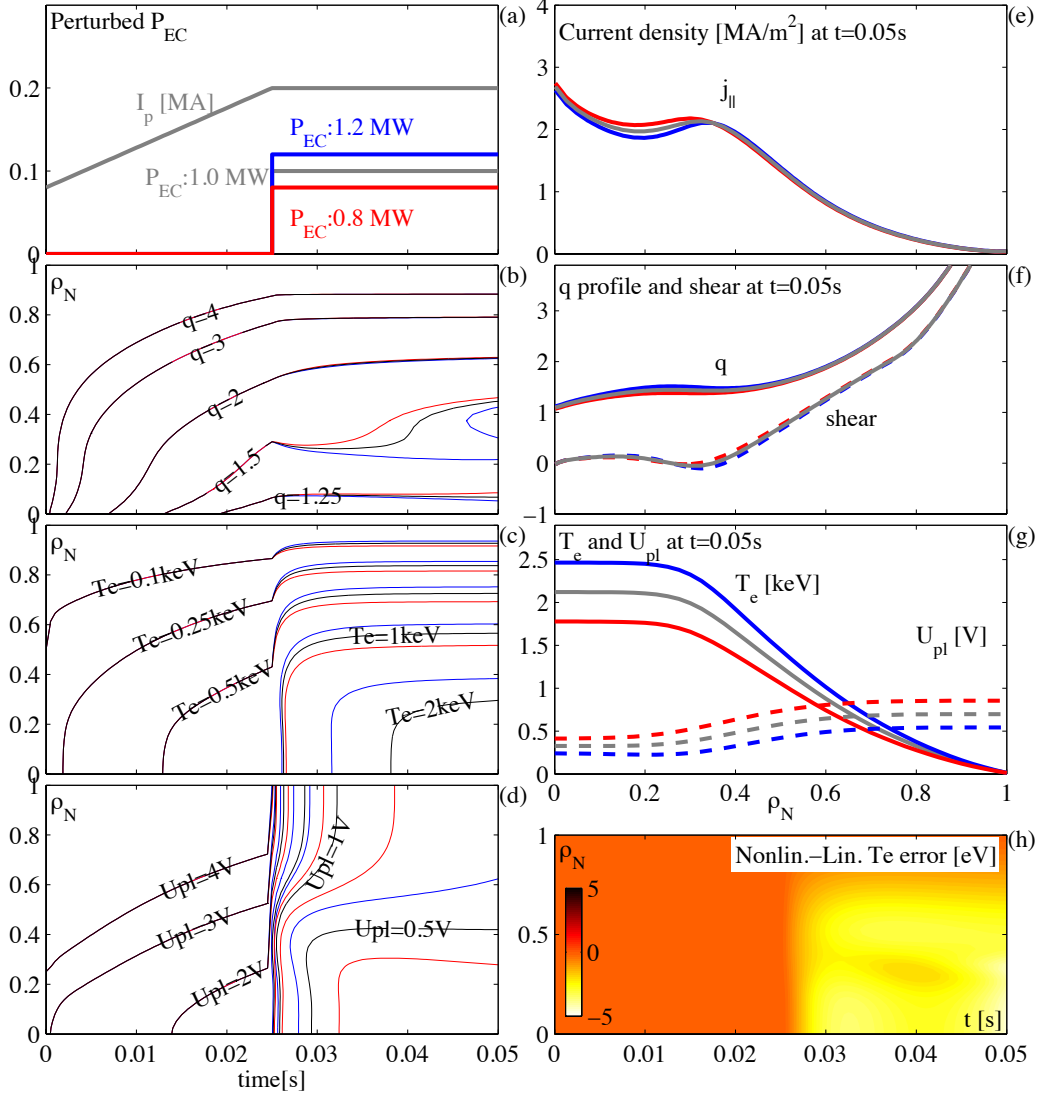

Figure 7.7: Perturbed profile trajectories for variations in the EC power level, calculated from the linearization of the nonlinear profile evolution shown in Figure 7.6. Gray curves show the nominal trajectories, while blue and red curves show, respectively, the trajectories for power variations of ± 200kW (a). The evolutions of constant q, T_e and U_{pl} surfaces is shown in (b),(c),(d), and the final profiles of $j_{\parallel}$, q, magnetic shear s, T_e and U_{pl} are given in (e),(f),(g). The error in T_e of the linearized trajectories (blue curve) with respect to a new nonlinear simulation with $P_{EC} = 1.2$MW is shown in (h).

7.5.4 Analysis of locally linearized profile dynamics

Let us consider another useful application of the knowledge of the Jacobian matrices, by further exploring the concept of local linearization and analyzing the linear models thus obtained.

Suppose an input actuator trajectory u_k^o (discrete-time notation is used) is given, then the profile state evolution x_k^o can be computed by Predictive-RAPTOR simulation. From knowledge of the Jacobian matrices, we can construct the local, linear model describing the linear dynamics of the profiles at a given time. The system is written in state-space form

$$\delta x_{k+1} = A_k \delta x_k + B_k \delta u_k \qquad (7.48)$$

where $\delta x_k = x_k - x_k^o$ and $\delta u_k = u_k - u_k^o$. Matrices A_k and B_k are obtained by linearizing (7.41) around (x_k^o, u_k^o). The linearization of the state equation $\tilde{f}(x_{k+1}^o, x_k^o, u_k^o) = 0$ (Eq.7.45) reads

$$0 = \frac{\partial \tilde{f}_k}{\partial x_{k+1}} \delta x_{k+1} + \frac{\partial \tilde{f}_k}{\partial x_k} \delta x_k + \frac{\partial \tilde{f}_k}{\partial u} \delta u_k \qquad (7.49)$$

where the Jacobians on the nominal trajectory $(x_{k+1}^o, x_k^o, u_k^o)$ have already been calculated for the Newton step, from which one recognizes

$$A_k = -\left(\frac{\partial \tilde{f}_k}{\partial x_{k+1}}\right)^{-1} \frac{\partial \tilde{f}_k}{\partial x_k}, \quad B_k = -\left(\frac{\partial \tilde{f}_k}{\partial x_{k+1}}\right)^{-1} \frac{\partial \tilde{f}_k}{\partial u_k} \qquad (7.50)$$

Note that $\frac{\partial \tilde{f}_k}{\partial x_{k+1}}$ is invertible in practice, a condition guaranteed by the existence of a unique solution of the physical problem. The model above is a **linear time-varying system**, consisting of a different linear model at each time step. A vast literature on these kind of systems exists, see for example (Khalil 2001).

To illustrate the diversity of behavior that is contained in this model, the dynamics of the linear systems obtained at each time step is studied. It should be stressed that such point-wise-in-time analysis of time-varying systems is by no means exhaustive and that other characteristics may be hidden. However this analysis highlights some of the fundamental difficulties in analyzing and studying the time-evolving tokamak profile dynamics from a control point of view.

The same plasma scenario and heating/current drive configuration is used as in the previous section, but this time the EC power is not increased step-wise but is gradually increased to its maximum (1MW) value. This provides a smoothly evolving plasma with increasing I_p and heating. The actuator trajectories and profile evolution at a number of instants during the evolution are shown in Figure 7.8(a)-(d). A standard method to visualize the dynamic behavior of a linear system is to plot its impulse response, i.e. the response of some system outputs to a delta function input (or a Kronecker delta, a single-sample pulse in the discrete domain). In the case of time-varying systems one will obtain time-varying impulse-response functions. The panels on the right show these impulse responses for pulses of I_p (Panels (e)-(h)) and P_{EC} (Panels (i)-(l)). Responses are shown of 4 different model outputs, from top to bottom the rotational transform at three radial locations $\rho = \{0, 0.3, 0.6\}$ and the central temperature T_{e0}.

The different impulse responses show dramatically different dynamic behavior as the plasma evolves from a cold low-temperature, low-current plasma to a hot, high temperature, high-current plasma. Not only does the response times become longer with increasing current diffusion time and confinement time, as is to be expected, but note also the initial negative response (known as non-minimum-phase behavior) of $\iota(\rho = 0)$ and $\iota(\rho = 0.3)$. Also, note the varying sign of the response for $\iota(\rho = 0.3)$ to an impulse in P_{EC}.
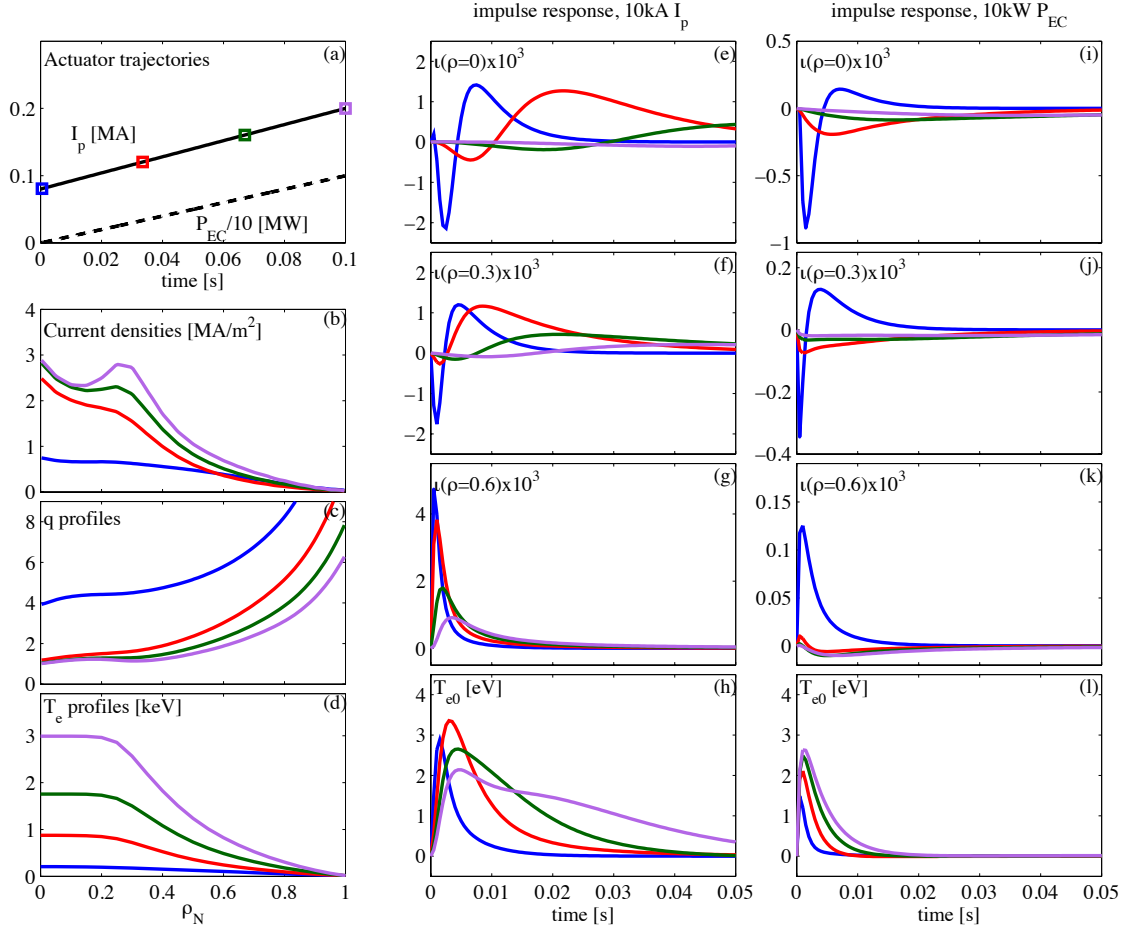

Figure 7.8: Impulse responses of local linear dynamic models at different times during a smooth plasma current and heating ramp-up. Actuator trajectories of I_p and $P_{EC}(\rho = 0.3)$ are shown in (a), profiles at indicated points in time are shown in (b)-(d). Impulse responses of ι (at radial locations $\rho = (0, 0.3, 0.6)$) and T_{e0} to: I_p (e)-(h) and P_{EC} (i)-(l) are shown. Different responses are visible depending on the state of the plasma.

Another way to visualize the variation in system dynamics is to plot the temporal evolution of the poles and zeros of the local linearizations. The poles are simply the eigenvalues of each A_k, while the zeros are the values of z for which the matrix $G_k(z) = C_k(Iz - A_k)B_k$ loses rank. In the complex z plane, poles z_p with absolute value smaller than 1 represent stable modes while $|z_p| > 1$ represents an unstable pole. The closer a pole is to $z = 1$, the longer the characteristic time scale. Unstable zeros, with $|z_0| > 1$ indicate non-minimum phase behavior, or initial undershoot, in linear systems and need to be taken into account in controller design.
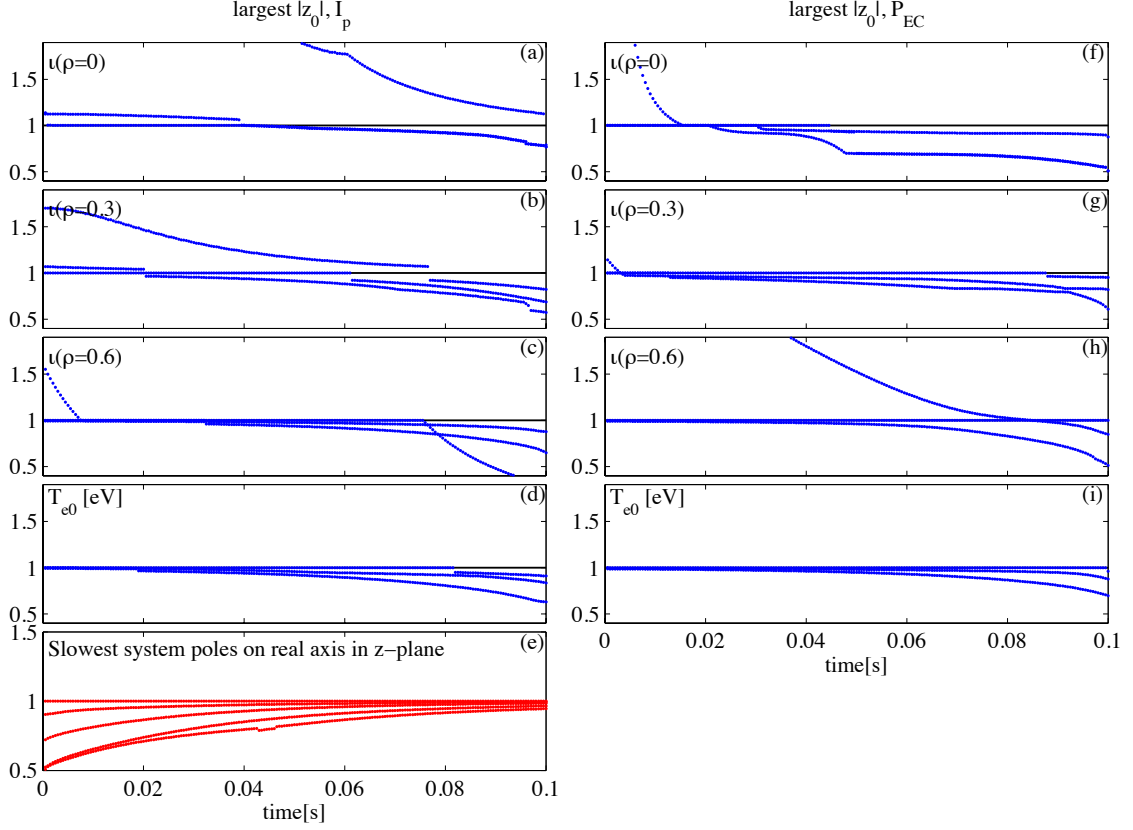
Figure 7.9: Loci of dominant zeros and poles of the linear models as a function of time. For the input-output channels corresponding to Fig.7.8 (e)-(h) and (i)-(l), the zeros with the largest absolute values are shown in, respectively, (a)-(d) and (f)-(i). Unstable zeros with $|z_0 > 1|$, corresponding to non-minimum phase behavior, transiently appear and disappear from the mappings. The system poles are shown in (e), and become slower (closer to 1) as the current diffusion time increases.

This diversity in dynamics, depending on time, highlights some of the pitfalls of a purely linear analysis of the profile dynamics. The foregoing analysis represents a first useful application of the Jacobians obtained in computing the nonlinear evolution. More details on the consequences for feedback controller design will be discussed in Section 9.5.3.

7.6 Outlook: extending the physics of RAPTOR

The RAPTOR code was designed from the outset to be a simple, lightweight transport code and never intended to contain the complete physics models of heavier codes which have taken decades of development to reach their present stage. Nevertheless, in this final section of the chapter some additional elements which could be added to RAPTOR, without denaturing it, will be enumerated. Recall that since the numerical integrations are performed using Newton steps, the derivatives of all the analytical expressions included in the model must be specified and handled through propagation of the chain rule. While not posing a conceptual problem, this complicates the development of additional modules.

7.6.1 Extending the kinetic profile transport models

At present only the electron temperature equation is evolved. However, since the structure of the transport equations for ions and for particle density are very similar, it would be a straightforward extension to simulate these profiles. This would be useful in some cases; in particular, if fusion power is to be included in the simulations which may be particularly interesting for ramp-down scenarios. When additional profiles are introduced, kinetic profile coupling via equipartition power and nonlinear terms involving density and temperature in the transport equations must be addressed. More complete transport expressions (including edge pedestals for H-mode scenarios) are possible as well, but it should be remembered that closed-form (differentiable) expressions are preferable, to avoid having to use (computationally intensive) finite difference schemes to obtain the derivatives of transport with respect to the profiles.

7.6.2 Time-dependent equilibrium

Including a time varying Grad-Shafranov equilibrium into RAPTOR can be done in two steps, of increasing complexity. In a first, simplified approach, a pre-computed time evolution of the shape can be used to extract geometric terms which vary in time. These geometric profiles can also be parametrized as a function of global shape parameters κ, δ, Shafranov shift and their temporal evolution prescribed instead. A second, approach is to self-consistently solve the Grad-Shafranov equation with the profile evolution as done in many other codes. Handling a time-varying equilibrium increases the number of time-varying terms in the model and therefore the computational complexity. This additional complexity must be weighed against the foreseen advantages.

7.6.3 Sawteeth, NTMs and other MHD

At present, RAPTOR excludes any MHD events such as sawteeth and tearing modes. These could be added quite simply by using crash-threshold models to trigger a reconnection (e.g. following the Porcelli model, see Chapter 3)), though care needs to be taken to properly propagate the parameter sensitivities across these discontinuous events. NTMs can likewise be modeled using the Modified Rutherford Equation (Section 4.2.1), and their effect on the confinement can be included.

In short, there are many opportunities for extending the range of physics covered by RAPTOR without excessive complexity. One must be careful however to include only the necessary equations in a given task, and one must bear in mind the original goal of the code: to provide a simple and fast transport model at the expense of completeness. As such, RAPTOR does not aspire to substitute or supersede existing codes, merely to complement them for specific tasks that have stringent speed constraints. Two such tasks are discussed in the coming chapters.

Bibliography

Albajar, F. et al. (2005). "Importance of electron cyclotron wave energy transport in ITER." In: *Nuclear Fusion* 45.7, p. 642. URL: http://stacks.iop.org/0029-5515/45/i=7/a=012.

Alberti, S. et al. (2005). "Third-harmonic, top-launch, ECRH experiments on TCV tokamak." In: *Nuclear Fusion* 45.11, pp. 1224–1231. URL: http://stacks.iop.org/0029-5515/45/1224.

Alberti, S. et al. (2011). "THz-Instrumentation development for gyrotron-DNP applications: from source to sample." In: *Third International Symposium on Dynamic Nuclear Polarization.* EPFL, Lausanne, Switzerland.

Ambrosino, G. and R. Albanese (2005). "Magnetic control of plasma current, position, and shape in Tokamaks: a survey or modeling and control approaches." In: *Control Systems, IEEE* 25.5, pp. 76 –92. ISSN: 1066-033X. DOI: 10.1109/MCS.2005.1512797.

Anderson, B.D.O. and J.B. Moore (1979). *Optimal filtering.* Mineola, NY (USA): Dover Publications.

Angioni, C. et al. (Feb. 2002). "Neutral beam stabilization of sawtooth oscillations in JET." In: *Plasma Physics and Controlled Fusion* 44, pp. 205–222. DOI: 10.1088/0741-3335/44/2/305.

Angioni, C. et al. (2003). "Effects of localized electron heating and current drive on the sawtooth period." In: *Nuclear Fusion* 43.6, pp. 455–468. URL: http://stacks.iop.org/0029-5515/43/455.

Ariola, M. and A. Pironti (2008). *Magnetic Control of Tokamak Plasmas.* Springer.

Artaud, J.F. et al. (2010). "The CRONOS suite of codes for integrated tokamak modelling." In: *Nuclear Fusion* 50.4, p. 043001. URL: http://stacks.iop.org/0029-5515/50/i=4/a=043001.

Artsimovich, L.A. (1972). "Tokamak devices." In: *Nuclear Fusion* 12.2, p. 215. URL: http://stacks.iop.org/0029-5515/12/i=2/a=012.

Åstrom, Karl J. and Björn Wittenmark (1997). *Computer-Controlled Systems: theory and design.* third. Upper Saddle River, New Jersey: Prentice Hall.

Barana, O. et al. (2007). "Integration of advanced feedback control techniques on Tore Supra." In: *Fusion Engineering and Design* 82.5-14. Proceedings of the 24th Symposium on Fusion Technology - SOFT-24, pp. 1023 –1029. ISSN: 0920-3796. DOI: DOI:10.1016/j.fusengdes.2007.05.054. URL: http://www.sciencedirect.com/science/article/pii/S0920379607002852.

Barry, S., C. Nieswand, and S.L. Prunty (1997). "Far-infrared polarimetry on the TCV tokamak." In: *Proceedings of the 8th international symposium on Laser-aided Plasma Diagnostics (LAPD-8).* Doorwerth, The Netherlands.

Barton, J. E. et al. (Nov. 2010). "Closed-Loop Simulation of Model-Based Current Profile Control with the DIII-D Plasma Control System." In: *APS Meeting Abstracts*, 9051P–+.

Berkel, M. van et al. (2011). "Real-time wavelet detection of crashes in limit cycles of non-stationary fusion plasmas." In: *Fusion Engineering and Design* In Press, Corrected Proof, pp. –. ISSN: 0920-3796. DOI: DOI:10.1016/j.fusengdes.2011.07.002. URL: http://www.sciencedirect.com/science/article/pii/S0920379611005084.

Berrino, J. et al. (2005). "Electron cyclotron emission temperature fluctuations associated with magnetic islands and real-time identification and control system." In: *Nuclear Fusion* 45.11, pp. 1350–1361. URL: http://stacks.iop.org/0029-5515/45/1350.

Blanchard, P et al. (2002). "High field side measurements of non-thermal electron cyclotron emission on TCV plasmas with ECH and ECCD." In: *Plasma Physics and Controlled Fusion* 44.10, p. 2231. URL: http://stacks.iop.org/0741-3335/44/i=10/a=310.

Blum, J. (1989). *Numerical Simulation and Optimal Control in Plasma Physics with Applications to Tokamaks.* Series in Modern Applied Mathematics. Paris: Wiley Gauthier-Villars.

Blum, J, C Boulbe, and B Faugeras (2008). "Real-time plasma equilibrium reconstruction in a Tokamak." In: *Journal of Physics: Conference Series* 135.1, p. 012019. URL: http://stacks.iop.org/1742-6596/135/i=1/a=012019.

Boozer, Allen H. (1998). "What is a stellarator?" In: 5.5, pp. 1647–1655. ISSN: 1070664X. DOI: DOI:10.1063/1.872833. URL: http://dx.doi.org/doi/10.1063/1.872833.

Bortolon, A. et al. (Dec. 2006). "Observation of Spontaneous Toroidal Rotation Inversion in Ohmically Heated Tokamak Plasmas." In: *Physical Review Letters* 97.23, pp. 235003–+. DOI: 10.1103/PhysRevLett.97.235003.

Breslau, J.A. et al. (2011). "Onset and saturation of a non-resonant internal mode in NSTX and implications for AT modes in ITER." In: *Nuclear Fusion* 51.6, p. 063027. URL: http://stacks.iop.org/0029-5515/51/i=6/a=063027.

Bryson, Arthur E. and Yu-Chi Ho (1975). *Applied Optimal Control.* New York: Taylor & Francis.

Budny, R.V. et al. (2008). "Predictions of H-mode performance in ITER." In: *Nuclear Fusion* 48.7, p. 075005. URL: http://stacks.iop.org/0029-5515/48/i=7/a=075005.

Burckhart, A et al. (2010). "Inter-ELM behaviour of the electron density and temperature pedestal in ASDEX Upgrade." In: *Plasma Physics and Controlled Fusion* 52.10, p. 105010. URL: http://stacks.iop.org/0741-3335/52/i=10/a=105010.

Burdakov, A V, A A Ivanov, and E P Kruglyakov (2010). "Modern magnetic mirrors and their fusion prospects." In: *Plasma Physics and Controlled Fusion* 52.12, p. 124026. URL: http://stacks.iop.org/0741-3335/52/i=12/a=124026.

Buttery, R. J. et al. (2002). "Neoclassical Tearing Physics in the Spherical Tokamak MAST." In: *Phys. Rev. Lett.* 88.12, p. 125005. DOI: 10.1103/PhysRevLett.88.125005.

Cacuci, Dan G. (1981). "Sensitivity theory for nonlinear systems. I. Nonlinear functional analysis approach." In: *Journal of Mathematical Physics* 22.12, pp. 2794–2802. DOI: 10.1063/1.525186. URL: http://link.aip.org/link/?JMP/22/2794/1.

Callen, D. et al. (1987). In: *Plasma Physics and Controlled Nuclear Fusion Research.* Vol. 2. Kyoto, Japan: IAEA, Vienna, p. 157.

Camenen, Y. et al. (2007a). "Current profile tailoring using localized electron cyclotron heating in highly elongated TCV plasmas." In: *Nuclear Fusion* 47, p. 586. DOI: 10.1088/0029-5515/47/7/010.

Camenen, Y. et al. (2007b). "Impact of plasma triangularity and collisionality on electron heat transport in TCV L-mode plasmas." In: *Nuclear Fusion* 47.7, pp. 510–516. URL: http://stacks.iop.org/0029-5515/47/510.

Camenen, Y. et al. (Dec. 2010). "Experimental demonstration of an up-down asymmetry effect on intrinsic rotation in the TCV tokamak." In: *Plasma Physics and Controlled Fusion* 52.12, pp. 124037–+. DOI: 10.1088/0741-3335/52/12/124037.

Canal, Gustavo (2011). "Coupling Between Sawteeth and Tearing Modes in TCV." In: *38th EPS Conference on Plasma Physics, 27 June - 1 July, Strasbourg, France.*

Carrera, R., R. D. Hazeltine, and M. Kotschenreuther (Apr. 1986). "Island bootstrap current modification of the nonlinear dynamics of the tearing mode." In: *Physics of Fluids* 29, pp. 899–902. DOI: 10.1063/1.865682.

Chapman, I T (2011). "Controlling sawtooth oscillations in tokamak plasmas." In: *Plasma Physics and Controlled Fusion* 53.1, p. 013001. URL: http://stacks.iop.org/0741-3335/53/i=1/a=013001.

Chapman, I T et al. (2007). "The physics of sawtooth stabilization." In: *Plasma Physics and Controlled Fusion* 49.12B, B385. URL: http://stacks.iop.org/0741-3335/49/i=12B/a=S35.

Chapman, I. T. et al. (Oct. 2010). "Empirical scaling of sawtooth period for onset of neoclassical tearing modes." In: *Nuclear Fusion* 50.10, pp. 102001–+. DOI: 10.1088/0029-5515/50/10/102001.

Chu, M S and M Okabayashi (2010). "Stabilization of the external kink and the resistive wall mode." In: *Plasma Physics and Controlled Fusion* 52.12, p. 123001. URL: http://stacks.iop.org/0741-3335/52/i=12/a=123001.

Cirant, S. et al. (2006). "Modulated ECCD experiments on TCV." In: *21th IAEA Fusion Energy Conference*. Paper EX/P3-3. Chengdu, China. URL: http://www-pub.iaea.org/MTCD/Meetings/Announcements.asp?ConfID=149,http://crpplocal.epfl.ch/pinboard/papers/068011201.pdf.

Coda, S et al. (2000). "High-power ECH and fully non-inductive operation with ECCD in the TCV tokamak." In: *Plasma Physics and Controlled Fusion* 42.12B, B311–B321. URL: http://stacks.iop.org/0741-3335/42/B311.

Coda, S. et al. (2003). "Electron cyclotron current drive and suprathermal electron dynamics in the TCV tokamak." In: *Nuclear Fusion* 43.11, pp. 1361–1370. URL: http://stacks.iop.org/0029-5515/43/1361.

Coda, S. et al. (2007). "The physics of electron internal transport barriers in the TCV tokamak." In: *Nuclear Fusion* 47.7, pp. 714–720. URL: http://stacks.iop.org/0029-5515/47/714.

Coda, S. et al. (2008). "Fully Bootstrap Discharge Sustainment in Steady State in the TCV Tokamak." In: *IAEA Conference 2008*. Geneva, Switzerland, EX/2–3.

Coda, S. and the TCV Team (2010). "Progress and Scientific Results in the TCV Tokamak." In: *23rd IAEA Fusion Energy Conference*. Daejon, Korea.

Connor, J.W. et al. (2004). "A review of internal transport barrier physics for steady-state operation of tokamaks." In: *Nuclear Fusion* 44.4, R1. URL: http://stacks.iop.org/0029-5515/44/i=4/a=R01.

Crotinger, J.A. et al. (1997). *UCRL-ID-126284*. Tech. rep. LLNL.

de Boor, C. (2001). *A Practical Guide to Splines*. Vol. 27. Applied Mathematical Science. Springer-Verlag, New York.

De Lazzari, D. and E. Westerhof (2009). "On the merits of heating and current drive for tearing mode stabilization." In: *Nuclear Fusion* 49.7, 075002 (8pp). URL: http://stacks.iop.org/0029-5515/49/075002.

de Vries, P. C. et al. (May 2011). "Survey of disruption causes at JET." In: *Nuclear Fusion* 51.5, pp. 053018–+. DOI: 10.1088/0029-5515/51/5/053018.

Decker, J and Y Peysson (2004). *Report EUR-CEA-FC-1736*. Tech. rep. Euratom-CEA.

Degeling, A. W. et al. (June 2003a). "ELM Dynamics in TCV H-modes." In: *Plasma Physics*. Ed. by I. S. Falconer, R. L. Dewar, & J. Khachan. Vol. 669. American Institute of Physics Conference Series, pp. 223–227. DOI: 10.1063/1.1593906.

Degeling, A. W. et al. (Sept. 2003b). "Magnetic triggering of ELMs in TCV." In: *Plasma Physics and Controlled Fusion* 45, pp. 1637–1655. DOI: 10.1088/0741-3335/45/9/306.

Donaldson, T. P. (Dec. 1978). "Theory of foil-absorption techniques for plasma X-ray continuum measurements." In: *Plasma Physics* 20, pp. 1279–1289. DOI: 10.1088/0032-1028/20/12/005.

Doyle, E.J. et al. (2007). "Chapter 2: Plasma confinement and transport." In: *Nuclear Fusion* 47.6, S18. URL: http://stacks.iop.org/0029-5515/47/i=6/a=S02.

Duval, B. P. et al. (2010). "Momentum Transport in TCV Across Sawteeth Events." In: *23rd IAEA Fusion Energy Conference*. Daejon, Korea.

Erba, M. et al. (1998). "Validation of a new mixed Bohm/gyro-Bohm model for electron and ion heat transport against the ITER, Tore Supra and START database discharges." In: *Nuclear Fusion* 38.7, p. 1013. URL: http://stacks.iop.org/0029-5515/38/i=7/a=305.

Esposito, B. et al. (2011). "Avoidance of disruptions at high β_N in ASDEX Upgrade with off-axis ECRH." In: *Nuclear Fusion* 51.8, p. 083051. URL: http://stacks.iop.org/0029-5515/51/i=8/a=083051.

Evans, T. E. et al. (June 2004). "Suppression of Large Edge-Localized Modes in High-Confinement DIII-D Plasmas with a Stochastic Magnetic Boundary." In: *Physical Review Letters* 92.23, pp. 235003–+. DOI: 10.1103/PhysRevLett.92.235003.

Fable, E et al. (2006). "Inward thermodiffusive particle pinch in electron internal transport barriers in TCV." In: *Plasma Physics and Controlled Fusion* 48.9, p. 1271. URL: http://stacks.iop.org/0741-3335/48/i=9/a=001.

Farina, D (2005). *GRAY: a quasi-optical ray tracing code for electron cyclotron absorption and current drive in tokamaks [PDF] from cnr.it*. Tech. rep. IFP-CNR Internal Report FP.

Favez, J-Y et al. (2005). "Improving tokamak vertical position control in the presence of power supply voltage saturation." In: *Plasma Physics and Controlled Fusion* 47.10, p. 1709. URL: http://stacks.iop.org/0741-3335/47/i=10/a=008.

Felici, F. (2011). *ECPOL: an object-oriented ECH polarization propagation code*. Tech. rep. CRPP.

Felici, F. et al. (2009a). "Real-time feedback control of millimeter-wave polarization for LHD." In: *Review of Scientific Instruments* 80.1, p. 013504. DOI: 10.1063/1.3073735.

Felici, F. et al. (2009b). "Self-consistent simulation of tearing modes during ECCD experiments on TCV." In: *36th EPS Conference on Plasma Physics, Sofia, Bulgaria, 29 June - 03 July.*

Felici, F. et al. (Oct. 2010a). "Feedback control of ECRH polarization on LHD." In: *Nuclear Fusion* 50.10, pp. 105003–+. DOI: 10.1088/0029-5515/50/10/105003.

Felici, F. et al. (Nov. 2010b). "RAPTOR: Optimization, real-time simulation and control of the tokamak q profile evolution using a simplified transport model." In: *APS Meeting Abstracts*, 9090P–+.

Felici, F. and O. Sauter (2011). "Nonlinear model-based optimization of actuator trajectories for tokamak plasma profile control." In: *Submitted to Plasma Physics and Controlled Fusion.*

Felici, F. et al. (2011a). "Optimization, real-time simulation and feedback control of tokamak plasma profiles on TCV." In: *38th EPS Conference on Plasma Physics, 27 June - 1 July, Strasbourg, France.*

Felici, F. et al. (2011b). "Real-time physics-model-based simulation of the current density profile in tokamak plasmas." In: *Nuclear Fusion* 51.8, p. 083052. URL: http://stacks.iop.org/0029-5515/51/i=8/a=083052.

Felton, R. et al. (2005). "Real-time measurement and control at JET experiment control." In: *Fusion Engineering and Design* 74.1-4. Proceedings of the 23rd Symposium of Fusion Technology - SOFT 23, pp. 561 –566. ISSN: 0920-3796. DOI: DOI:10.1016/j.fusengdes.2005.06.286. URL: http://www.sciencedirect.com/science/article/pii/S0920379605003352.

Ferron, J.R. et al. (1998). "Real time equilibrium reconstruction for tokamak discharge control." In: *Nuclear Fusion* 38.7, p. 1055. URL: http://stacks.iop.org/0029-5515/38/i=7/a=308.

Ferron, J.R. et al. (2006). "Feedback control of the safety factor profile evolution during formation of an advanced tokamak discharge." In: *Nuclear Fusion* 46, p. L13. DOI: 10.1088/0029-5515/46/10/L01.

Firestone, M.A. and C.E. Kessel (1991a). "Electromagnetac And Kinetic Control Of A Tokamak Reactor." In: *Plasma Science, 1991. IEEE Conference Record - Abstracts., 1991 IEEE International Conference on*, pp. 193 –194. DOI: 10.1109/PLASMA.1991.695738.

— (1991b). "Plasma kinetic control in a tokamak." In: *Plasma Science, IEEE Transactions on* 19.1, pp. 29 –41. ISSN: 0093-3813. DOI: 10.1109/27.62364.

Fitzpatrick, Richard (1995). "Helical temperature perturbations associated with tearing modes in tokamak plasmas." In: *Physics of Plasmas* 2.3, pp. 825–838.

Franke, Stefan (1997). "Application of Thomson scattering at 1.06mm as a diagnostic for spatial profile measurements of electron temperature and density on the TCV tokamak." PhD thesis. Lausanne, Switzerland: EPFL.

Franklin, Gene F and J. David Powell (2002). *Feedback control of dynamic systems*. fourth. Upper Saddle River, New Jersey: Prentice Hall.

Friedberg, Jeffrey P. (1987). *Ideal Magnetohydrodynamics*. Modern perspectives in energy. 233 Spring Street, New York: Plenum Press. ISBN: 0-306-42512-2.

Fujita, T. et al. (2001). "Quasisteady High-Confinement Reversed Shear Plasma with Large Bootstrap Current Fraction under Full Noninductive Current Drive Condition in JT-60U." In: *Phys. Rev. Lett.* 87.8, p. 085001. DOI: 10.1103/PhysRevLett.87.085001.

Fujita, T. and the JT-60 team (2006). "Steady state operation research in JT-60U with extended pulse length." In: *Nuclear Fusion* 46.3, S3. URL: http://stacks.iop.org/0029-5515/46/i=3/a=S02.

Fujita, Takaaki (2010). "Tokamak equilibria with nearly zero central current: the current hole." In: *Nuclear Fusion* 50.11, p. 113001. URL: http://stacks.iop.org/0029-5515/50/i=11/a=113001.

Furth, Harold P., John Killeen, and Marshall N. Rosenbluth (1963). "Finite-Resistivity Instabilities of a Sheet Pinch." In: *Physics of Fluids* 6.4, pp. 459–484. DOI: 10.1063/1.1706761. URL: http://link.aip.org/link/?PFL/6/459/1.

Furth, H.P., P.H. Rutherford, and H. Selberg (1973). "Tearing mode in the cylindrical tokamak." In: *The Physics of Fluids* 16.7, pp. 1054–1063.

Gantenbein, G. et al. (2000). "Complete Suppression of Neoclassical Tearing Modes with Current Drive at the Electron-Cyclotron-Resonance Frequency in ASDEX Upgrade Tokamak." In: *Phys. Rev. Lett.* 85.6, pp. 1242–1245. DOI: 10.1103/PhysRevLett.85.1242.

Garcia, J. and G. Giruzzi (May 2010). "Critical Behavior of Magnetically Confined Plasma Regimes." In: *Physical Review Letters* 104.20, pp. 205003–+. DOI: 10.1103/PhysRevLett.104.205003.

Genacchi, G. and A. Taroni (1988). *JETTO: a free boundary plasma transport code.* RT/TIB 5. ENEA.

Glasser, A. H., J. M. Greene, and J. L. Johnson (1975). "Resistive instabilities in general toroidal plasma configurations." In: *Physics of Fluids* 18.7, pp. 875–888. DOI: 10.1063/1.861224. URL: http://link.aip.org/link/?PFL/18/875/1.

Goedbloed, J.P. and S. Poedts (2004). *Principles of Magnetohydrodynamics; with Applications to Laboratory and Astrophysical Plasmas.* Cambridge: Cambridge University Press.

Goedbloed, J.P., R. Keppens, and S. Poedts (2010). *Advanced Magnetohydrodynamics; with Applications to Laboratory and Astrophysical Plasmas.* Cambridge: Cambridge University Presserity Press.

Goeler, S. von, W. Stodiek, and N. Sauthoff (1974). "Studies of Internal Disruptions and $m = 1$ Oscillations in Tokamak Discharges with Soft—X-Ray Tecniques." In: *Phys. Rev. Lett.* 33.20, pp. 1201–1203. DOI: 10.1103/PhysRevLett.33.1201.

Golub, Gene H. and Charles F. Van Loan (1996). *Matrix Computations.* ISBN: 0-8018-5413-X. London, UK: The Johns Hopkins University Press.

Goodman, T P et al. (2005). "Safety factor profile requirements for electron ITB formation in TCV." In: *Plasma Physics and Controlled Fusion* 47.12B, B107–B120. URL: http://stacks.iop.org/0741-3335/47/B107.

Goodman, T. P. and the TCV team (May 2008). "Experience in integrated control of the multi-megawatt electron cyclotron heating system on the TCV tokamak: the first decade." In: *Nuclear Fusion* 48.5, pp. 054011–+. DOI: 10.1088/0029-5515/48/5/054011.

Goodman, T. P. et al. (2008). "First measurements of oblique ECE with a real-time movable line of sight on TCV." In: *FUSION SCIENCE AND TECHNOLOGY* 53.1. 14th Joint Workshop on Electron Cyclotron Emission and Electron Cyclotron Resonance Heating, Santorini, GREECE, MAY 09-12, 2006, 196–207. ISSN: 1536-1055.

Goodman, T. P. et al. (June 2011). "Sawtooth Pacing by Real-Time Auxiliary Power Control in a Tokamak Plasma." In: *Physical Review Letters* 106.24, pp. 245002–+. DOI: 10.1103/PhysRevLett.106.245002.

Goodman, T.P. et al. (2007). "Co- and Counter - viewing oblique ECE measurements during ECH and ECCD on the TCV tokamak." In: *34th EPS Conference on Plasma Physics, Warsaw Congress Centre, Poland, 02 July 2007*.

Gormezano, C et al. (2004). "Hybrid advanced scenarios: perspectives for ITER and new experiments with dominant RF heating." In: *Plasma Physics and Controlled Fusion* 46.12B, B435. URL: http://stacks.iop.org/0741-3335/46/i=12B/a=037.

Gormezano, C. et al. (2007). "Chapter 6: Steady state operation." In: *Nuclear Fusion* 47.6, S285. URL: http://stacks.iop.org/0029-5515/47/i=6/a=S06.

Grad, H. and H. Rubin (1958). "Hydromagnetic Equilibria and Force-Free Fields." In: *Proceedings of the 2nd UN Conf. on the Peaceful Uses of Atomic Energy*. Vol. 31. IAEA. Geneva, p. 190.

Graves, J P et al. (2005). "Sawtooth control in fusion plasmas." In: *Plasma Physics and Controlled Fusion* 47.12B, B121–B133. URL: http://stacks.iop.org/0741-3335/47/B121.

Graves, J. P. et al. (2009). "Sawtooth-Control Mechanism using Toroidally Propagating Ion-Cyclotron-Resonance Waves in Tokamaks." In: *Phys. Rev. Lett.* 102.6, p. 065005. DOI: 10.1103/PhysRevLett.102.065005.

Grigorenko, Ilya (2006). *Optimal Control And Forecasting of Complex Dynamical Systems*. World Scientific Publishing Company.

Hammett, Gregory W. and Francis W. Perkins (1990). "Fluid moment models for Landau damping with application to the ion-temperature-gradient instability." In: *Phys. Rev. Lett.* 64.25, pp. 3019–3022. DOI: 10.1103/PhysRevLett.64.3019.

Harvey, R. W. et al. (May 2002). "Radial Transport and Electron-Cyclotron-Current Drive in the TCV and DIII-D Tokamaks." In: *Physical Review Letters* 88.20, pp. 205001–+. DOI: 10.1103/PhysRevLett.88.205001.

Hawryluk, R J (1980). In: *Physics of Plasmas Close to Thermonuclear Conditions*. Ed. by B. Coppi. Vol. 1, p. 19.

Haykin, S. (1999). *Neural Networks: A Comprehensive Foundation, second edition*. Second. Upper Saddle River, New Jersey: Prentice Hall.

Hegna, C. C. (1998). "The physics of neoclassical magnetohydrodynamic tearing modes." In: *Physics of Plasmas* 5.5, pp. 1767–1774. DOI: 10.1063/1.872846. URL: http://link.aip.org/link/?PHP/5/1767/1.

Hender, T.C. et al. (2007). "Chapter 3: MHD stability, operational limits and disruptions." In: *Nuclear Fusion* 47.6, S128–S202. URL: http://stacks.iop.org/0029-5515/47/S128.

Henderson, M. A. et al. (2004). "Rapid and Localized Electron Internal-Transport-Barrier Formation During Shear Inversion in Fully Noninductive TCV Discharges." In: *Physical Review Letters* 93.21, 215001, p. 215001. DOI: 10.1103/PhysRevLett.93.215001. URL: http://link.aps.org/abstract/PRL/v93/e215001.

Hennen, B A et al. (2010). "Real-time control of tearing modes using a line-of-sight electron cyclotron emission diagnostic." In: *Plasma Physics and Controlled Fusion* 52.10, p. 104006. URL: http://stacks.iop.org/0741-3335/52/i=10/a=104006.

Hinton, F. L. and R. D. Hazeltine (1976). "Theory of plasma transport in toroidal confinement systems." In: *Rev. Mod. Phys.* 48.2, pp. 239–308. DOI: 10.1103/RevModPhys. 48.239.

Hofmann, F. (1988). "FBT - a free-boundary tokamak equilibrium code for highly elongated and shaped plasmas." In: *Computer Physics Communications* 48.2, pp. 207 – 221. ISSN: 0010-4655. DOI: DOI:10.1016/0010-4655(88)90041-0. URL: http://www.sciencedirect.com/science/article/B6TJ5-46DF8X2-37/2/a7064d1131afc8b1fdecd3bbaa41a177.

Hofmann, F. and G. Tonetti (1988). "Tokamak equilibrium reconstruction using faraday rotation measurements." In: *Nuclear Fusion* 28.10, p. 1871.

Hofmann, F. and S.C. Jardin (1990). "Plasma shape and position control in highly elongated tokamaks." In: *Nuclear Fusion* 30.10, p. 2013. URL: http://stacks.iop.org/0029-5515/30/i=10/a=003.

Hofmann, F et al. (1994). "Creation and control of variably shaped plasmas in TCV." In: *Plasma Physics and Controlled Fusion* 36.12B, B277. URL: http://stacks.iop.org/0741-3335/36/i=12B/a=023.

Hofmann, F. et al. (1998). "Feedback stabilization of axisymmetric modes in the TCV tokamak using active coils inside and outside the vacuum vessel." In: *Nuclear Fusion* 38.3, p. 399. URL: http://stacks.iop.org/0029-5515/38/i=3/a=306.

Hofmann, F. et al. (2000). "Vertical position control in TCV: Comparison of model predictions with experimental results." In: *Nuclear Fusion* 40.4, p. 767. URL: http://stacks.iop.org/0029-5515/40/i=4/a=302.

Hofmann, F et al. (2001). "Stability and energy confinement of highly elongated plasmas in TCV." In: *Plasma Physics and Controlled Fusion* 43.12A, A161. URL: http://stacks.iop.org/0741-3335/43/i=12A/a=312.

Horton, L D et al. (2004). "ITER-relevant H-mode physics at ASDEX Upgrade." In: *Plasma Physics and Controlled Fusion* 46.12B, B511. URL: http://stacks.iop.org/0741-3335/46/i=12B/a=042.

Hughes, Thomas J. R. (1987). *The finite element method.* New Jersey, USA: Prentice Hall.

Humphreys, D. A. et al. (2006). "Active control for stabilization of neoclassical tearing modes." In: *Physics of Plasmas* 13.5, 056113, p. 056113. DOI: 10.1063/1.2173606. URL: http://link.aip.org/link/?PHP/13/056113/1.

Humphreys, D.A. et al. (2007). "Development of ITER-relevant plasma control solutions at DIII-D." In: *Nuclear Fusion* 47.8, p. 943. URL: http://stacks.iop.org/0029-5515/47/i=8/a=028.

Imbeaux, F. et al. (2011a). "Current ramps in tokamaks: from present experiments to ITER scenarios." In: *Nuclear Fusion* 51.8, p. 083026. URL: http://stacks.iop.org/0029-5515/51/i=8/a=083026.

Imbeaux, F. et al. (2011b). "Real-time control of the safety factor profile diagnosed by magneto-hydrodynamic activity on the Tore Supra tokamak." In: *Nuclear Fusion* 51.7, p. 073033. URL: http://stacks.iop.org/0029-5515/51/i=7/a=073033.

Isayama, A et al. (2000). "Complete stabilization of a tearing mode in steady state high-β_p H-mode discharges by the first harmonic electron cyclotron heating/current drive on JT-60U." In: *Plasma Physics and Controlled Fusion* 42.12, p. L37. URL: http://stacks.iop.org/0741-3335/42/i=12/a=102.

Isayama, A. et al. (2007). "Stabilization of neoclassical tearing modes by electron cyclotron current drive in JT-60U." In: *Nuclear Fusion* 47.8, p. 773. URL: http://stacks.iop.org/0029-5515/47/i=8/a=007.

Isayama, A. et al. (2009). "Neoclassical tearing mode control using electron cyclotron current drive and magnetic island evolution in JT-60U." In: *Nuclear Fusion* 49.5, p. 055006. URL: http://stacks.iop.org/0029-5515/49/i=5/a=055006.

Jacquinot, J. and the JET team (Mar. 1999). "Deuterium-tritium operation in magnetic confinement experiments: results and underlying physics." In: *Plasma Physics and Controlled Fusion* 41, A13–A46.

Jardin, S. C., N. Pomphrey, and J. Delucia (1986). "Dynamic modeling of transport and positional control of tokamaks." In: *Journal of Computational Physics* 66.2, pp. 481 –507. ISSN: 0021-9991. DOI: DOI:10.1016/0021-9991(86)90077-X. URL: http://www.sciencedirect.com/science/article/pii/002199918690077X.

Jardin, S.C., M.G. Bell, and N. Pomphrey (1993). "TSC simulation of Ohmic discharges in TFTR." In: *Nuclear Fusion* 33.3, p. 371. URL: http://stacks.iop.org/0029-5515/33/i=3/a=I01.

Jenkins, Thomas G. et al. (2010). "Calculating electron cyclotron current drive stabilization of resistive tearing modes in a nonlinear magnetohydrodynamic model." In: *Physics of Plasmas* 17.1, 012502, p. 012502. DOI: 10.1063/1.3276740. URL: http://link.aip.org/link/?PHP/17/012502/1.

Joffrin, E et al. (2003). "Integrated scenario in JET using real-time profile control." In: *Plasma Physics and Controlled Fusion* 45.12A, A367. URL: http://stacks.iop.org/0741-3335/45/i=12A/a=024.

Joffrin, E. et al. (July 2005). "The 'hybrid' scenario in JET: towards its validation for ITER." In: *Nuclear Fusion* 45, pp. 626–634. DOI: 10.1088/0029-5515/45/7/010.

Joffrin, E. et al. (2007). "Integrated plasma controls for steady state scenarios." In: *Nuclear Fusion* 47.12, p. 1664. URL: http://stacks.iop.org/0029-5515/47/i=12/a=004.

Joffrin, E. et al. (2010). "High confinement hybrid scenario in JET and its significance for ITER." In: *23rd IAEA Fusion Energy Conference, Daejon, Korea*. IAEA-CN-165/EX/1-1. Daejon, South Korea.

Khalil, Hassan K. (2001). *Nonlinear Systems*. 3rd ed. Prentice-Hall, Inc.

Khayrutdinov, R. R. and V. E. Lukash (1993). "Studies of Plasma Equilibrium and Transport in a Tokamak Fusion Device with the Inverse-Variable Technique." In: *Journal of Computational Physics* 109.2, pp. 193 –201. ISSN: 0021-9991. DOI: DOI:10.1006/jcph.1993.1211. URL: http://www.sciencedirect.com/science/article/pii/S0021999183712118.

Kim, S. H. et al. (Oct. 2009). "Full tokamak discharge simulation of ITER by combining DINA-CH and CRONOS." In: *Plasma Physics and Controlled Fusion* 51.10, pp. 105007–+. DOI: 10.1088/0741-3335/51/10/105007.

Klimanov, I. et al. (2005). "Electron cyclotron emission spectrometry on the Tokamak à Configuration Variable." In: 76.9, p. 093504. ISSN: 00346748. DOI: DOI:10.1063/1.2042667. URL: http://dx.doi.org/doi/10.1063/1.2042667.

Klimanov, I. et al. (Mar. 2007). "BRIEF COMMUNICATION: Generation of suprathermal electrons during sawtooth crashes in a tokamak plasma." In: *Plasma Physics and Controlled Fusion* 49, pp. 1–+. DOI: 10.1088/0741-3335/49/3/L01.

Koslowski, H.R. et al. (2001). "MHD studies in radiating mantle plasmas on JET." In: *21st EPS Conference on Plasma Physics, Funchal (PT), 18-22 June*.

Kritz, A.H. et al. (1982). In: *Proc. 3rd Int. Symp. on Heating in Toroidal Plasmas*. Vol. II. Brussels, p. 707.

La Haye, R. J. (2006). "Neoclassical tearing modes and their control." In: *Physics of Plasmas* 13.5, 055501, p. 055501. DOI: 10.1063/1.2180747. URL: http://link.aip.org/link/?PHP/13/055501/1.

La Haye, R. J. and O. Sauter (July 1998). "Threshold for metastable tearing modes in DIII-D." In: *Nuclear Fusion* 38, pp. 987–999. DOI: 10.1088/0029-5515/38/7/303.

La Haye, R.J. et al. (2005). "Higher stable beta by use of pre-emptive electron cyclotron current drive on DIII-D." In: *Nuclear Fusion* 45.11, p. L37. URL: http://stacks.iop.org/0029-5515/45/i=11/a=L02.

La Haye, R.J. et al. (2006). "Cross–machine benchmarking for ITER of neoclassical tearing mode stabilization by electron cyclotron current drive." In: *Nuclear Fusion* 46.4, p. 451. URL: http://stacks.iop.org/0029-5515/46/i=4/a=006.

La Haye, R.J., A. Isayama, and M. Maraschek (2009). "Prospects for stabilization of neoclassical tearing modes by electron cyclotron current drive in ITER." In: *Nuclear Fusion* 49.4, p. 045005. URL: http://stacks.iop.org/0029-5515/49/i=4/a=045005.

Lang, P. T. et al. (May 2004). "ELM pace making and mitigation by pellet injection in ASDEX Upgrade." In: *Nuclear Fusion* 44, pp. 665–677. DOI: 10.1088/0029-5515/44/5/010.

Lauret, M. et al. (2011). "Demonstration of sawtooth period locking with power modulation in TCV plasmas." In: *Submitted to Physical Review Letters*.

Lazarus, E.A., J.B. Lister, and G.H. Neilson (1990). "Control of the vertical instability in tokamaks." In: *Nuclear Fusion* 30.1, p. 111. URL: http://stacks.iop.org/0029-5515/30/i=1/a=010.

Lazzari, D. De and E. Westerhof (2010). "On the merits of heating and current drive for tearing mode stabilization." In: *Nuclear Fusion* 50.7, p. 079801. URL: http://stacks.iop.org/0029-5515/50/i=7/a=079801.

Lennholm, M. et al. (2009). "Demonstration of Effective Control of Fast-Ion-Stabilized Sawteeth by Electron-Cyclotron Current Drive." In: *Phys. Rev. Lett.* 102.11, p. 115004. DOI: 10.1103/PhysRevLett.102.115004.

Lennholm, M. et al. (July 2011). "Feedback control of the sawtooth period through real time control of the ion cyclotron resonance frequency." In: *Nuclear Fusion* 51.7, pp. 073032–+. DOI: 10.1088/0029-5515/51/7/073032.

Lindl, J. D. and E. I. Moses (May 2011). "Special Topic: Plans for the National Ignition Campaign (NIC) on the National Ignition Facility (NIF): On the threshold of initiating ignition experiments." In: *Physics of Plasmas* 18.5, pp. 050901–+. DOI: 10.1063/1.3591001.

Lister, J.B. et al. (1997). "The control of tokamak configuration variable plasmas." In: *Fusion Technology* 32.3. cited By (since 1996) 32, pp. 321–373. URL: http://www.scopus.com/inward/record.url?eid=2-s2.0-0031272843&partnerID=40&md5=46edddea076f5d52ea558debbe6baec0.

Ljung, Lennart (1999). *System Identification, Theory for the User*. Second. Upper Saddle River, New Jersey: Prentice-Hall. ISBN: 0-13-656695-2.

Luce, T. C. et al. (2004). "High performance stationary discharges in the DIII-D tokamak." In: *Physics of Plasmas* 11.5, pp. 2627–2636. DOI: 10.1063/1.1704644. URL: http://link.aip.org/link/?PHP/11/2627/1.

Lutjens, H., A. Bondeson, and O. Sauter (1996). "The CHEASE code for toroidal MHD equilibria." In: *Computer Physics Communications* 97.3, pp. 219–260. ISSN: 0010-4655. DOI: 10.1016/0010-4655(96)00046-X.

Lütjens, Hinrich, Jean-François Luciani, and Xavier Garbet (2001). "Curvature effects on the dynamics of tearing modes in tokamaks." In: 8.10, pp. 4267–4270. ISSN: 1070664X. DOI: DOI:10.1063/1.1399056. URL: http://dx.doi.org/doi/10.1063/1.1399056.

Lyon, J.F. et al. (1990). "Stellarators." In: *Nuclear Fusion* 30.9, p. 1695. URL: http://stacks.iop.org/0029-5515/30/i=9/a=004.

Maget, P. et al. (2010). "Modelling of (2,1) NTM threshold in JET advanced scenarios." In: *Nuclear Fusion* 50.4, p. 045004. URL: http://stacks.iop.org/0029-5515/50/i=4/a=045004.

Maraschek, M et al. (2003). "Scaling of the marginal β_p of neoclassical tearing modes during power ramp-down experiments in ASDEX Upgrade." In: *Plasma Physics and Controlled Fusion* 45.7, p. 1369. URL: http://stacks.iop.org/0741-3335/45/i=7/a=322.

Maraschek, M. et al. (2005). "Active control of MHD instabilities by ECCD in ASDEX Upgrade." In: *Nuclear Fusion* 45.11, pp. 1369–1376. URL: http://stacks.iop.org/0029-5515/45/1369.

Maraschek, M. et al. (2007). "Enhancement of the Stabilization Efficiency of a Neoclassical Magnetic Island by Modulated Electron Cyclotron Current Drive in the ASDEX Upgrade Tokamak." In: *Physical Review Letters* 98.2, 025005, p. 025005. URL: http://link.aps.org/abstract/PRL/v98/e025005.

Martin, Y. R., A. W. Degeling, and J. B. Lister (May 2002). "Search for determinism in ELM time series in TCV." In: *Plasma Physics and Controlled Fusion* 44.26, A260000–A382.

Martin, Y. R. et al. (Dec. 2003). "Accessibility and properties of ELMy H-mode and ITB plasmas in TCV." In: *Plasma Physics and Controlled Fusion* 45.26, A260000–A365. DOI: 10.1088/0741-3335/45/12A/023.

Martin, Y. R., L. Porte, and S. Alberti (May 2006). "Third harmonic EC heating of ELMy H-mode in TCV." In: *Plasma Physics and Controlled Fusion* 48.26, A260000–A169. DOI: 10.1088/0741-3335/48/5A/S15.

Matsuda, K. (Feb. 1989). "Ray tracing study of the electron cyclotron current drive in DIII-D using 60 GHz." In: *IEEE Transactions on Plasma Science* 17, pp. 6–11. DOI: 10.1109/27.21664.

Moreau, D. and I. Voitsekhovitch (1999). "Plasma control issues for an advanced steady state tokamak reactor." In: *Nuclear Fusion* 39.5, p. 685. URL: http://stacks.iop.org/0029-5515/39/i=5/a=308.

Moreau, D. et al. (2008). "A two-time-scale dynamic-model approach for magnetic and kinetic profile control in advanced tokamak scenarios on JET." In: *Nuclear Fusion* 48.10, p. 106001. URL: http://stacks.iop.org/0029-5515/48/i=10/a=106001.

Moreau, D. et al. (2011). "Plasma models for real-time control of advanced tokamak scenarios." In: *Nuclear Fusion* 51.6, p. 063009. URL: http://stacks.iop.org/0029-5515/51/i=6/a=063009.

Moret, J.-M. et al. (1997). "Influence of Plasma Shape on Transport in the TCV Tokamak." In: *Phys. Rev. Lett.* 79.11, pp. 2057–2060. DOI: 10.1103/PhysRevLett.79.2057.

Moret, J.-M. et al. (June 1998). "Magnetic measurements on the TCV Tokamak." In: *Review of Scientific Instruments* 69, pp. 2333–2348. DOI: 10.1063/1.1148940.

Morrow-Jones, J. et al. (1993). "Use of tokamak dynamics models for digital filtering and control." In: *Fusion Engineering, 1993., 15th IEEE/NPSS Symposium on.* Vol. 1, 219 –222 vol.1. DOI: 10.1109/FUSION.1993.518318.

Mueck, A. et al. (Apr. 2007). "Demonstration of Electron-Bernstein-Wave Heating in a Tokamak via O-X-B Double-Mode Conversion." In: *Physical Review Letters* 98.17, pp. 175004–+. DOI: 10.1103/PhysRevLett.98.175004.

Murari, A. et al. (2009). "Unbiased and non-supervised learning methods for disruption prediction at JET." In: *Nuclear Fusion* 49.5, p. 055028. URL: http://stacks.iop.org/0 029-5515/49/i=5/a=055028.

Nave, M.F.F. and J.A. Wesson (1990). "Mode locking in tokamaks." In: *Nuclear Fusion* 30.12, p. 2575. URL: http://stacks.iop.org/0029-5515/30/i=12/a=011.

Nikkola, P. et al. (Nov. 2003). "Modelling of the electron cyclotron current drive experiments in the TCV tokamak." In: *Nuclear Fusion* 43, pp. 1343–1352. DOI: 10.1088/00 29-5515/43/11/006.

Nocedal, Jorge and Stephen Wright (2006). *Numerical Optimization.* Second. Springer Series in Operations Research and Financial Engineering. Springer.

Ogata, K. (2002). *Modern Control Systems.* 4th. Prentice Hall.

Oikawa, T. et al. (2005). "Evolution of the Current Density Profile Associated with Magnetic Island Formation in JT-60U." In: *Physical Review Letters* 94. DOI: 10.11 03/PhysRevLett.94.125003.

Oosterbeek, J. W. et al. (Sept. 2008). "A line-of-sight electron cyclotron emission receiver for electron cyclotron resonance heating feedback control of tearing modes." In: *Review of Scientific Instruments* 79.9, pp. 093503–+. DOI: 10.1063/1.2976665.

Ou, Y. et al. (2007). "Towards model-based current profile control at DIII-D." In: *Fusion Engineering and Design* 82.5-14. Proceedings of the 24th Symposium on Fusion Technology - SOFT-24, pp. 1153 –1160. ISSN: 0920-3796. DOI: DOI:10.1016/j.fusengdes.20 07.04.016. URL: http://www.sciencedirect.com/science/article/B6V3C-4NYBMFM-1/2/fa0bf0cc42e00f56a0dca3a2e4fb68e8.

Ou, Y et al. (2008). "Design and simulation of extremum-seeking open-loop optimal control of current profile in the DIII-D tokamak." In: *Plasma Physics and Controlled Fusion* 50.11, 115001 (24pp). URL: http://stacks.iop.org/0741-3335/50/115001.

Ou, Y. et al. (2010a). "Optimal Tracking Control of Current Profile in Tokamaks." In: *Control Systems Technology, IEEE Transactions on.* ISSN: 1063-6536. DOI: 10.110 9/TCST.2010.2046640.

Ou, Yongsheng, Chao Xu, and E. Schuster (2010b). "Robust Control Design for the Poloidal Magnetic Flux Profile Evolution in the Presence of Model Uncertainties." In: *Plasma Science, IEEE Transactions on* 38.3, pp. 375 –382. ISSN: 0093-3813. DOI: 10.1109/TPS.2009.2038476.

Ouarit, H. et al. (2011). "Validation of plasma current profile model predictive control in tokamaks via simulations." In: *Fusion Engineering and Design* In Press, Corrected Proof, pp. –. ISSN: 0920-3796. DOI: DOI:10.1016/j.fusengdes.2011.03.078. URL: http://www.sciencedirect.com/science/article/B6V3C-52NSTY4-3/2/2d9a19f1eb1cd 2c72c8fa4815bb1e893.

Paley, J I, S Coda, and the TCV Team (2007). "Real time control of the plasma current and elongation in tokamaks using ECRH actuators." In: *Plasma Physics and Controlled Fusion* 49.10, pp. 1735–1746. URL: http://stacks.iop.org/0741-3335/49/1735.

Paley, J. I. et al. (2009). "From profile to sawtooth control: developing feedback control using ECRH/ECCD systems on the TCV tokamak." In: *Plasma Physics and Controlled Fusion* 51.12, 124041 (11pp). URL: http://stacks.iop.org/0741-3335/51/124041.

Paley, J. I. et al. (May 2009). "Real time control of the sawtooth period using EC launchers." In: *Plasma Physics and Controlled Fusion* 51.5, pp. 055010–+. DOI: 10.1088/0741-3335/51/5/055010.

Paley, J.I. et al. (2010). "Architecture and commissioning of the TCV distributed feedback control system." In: *17th IEEE-NPSS Real Time Conference (RT)*, pp. 1 –6. DOI: 10.1109/RTC.2010.5750487.

Pankin, Alexei et al. (2004). "The tokamak Monte Carlo fast ion module NUBEAM in the National Transport Code Collaboration library." In: *Computer Physics Communications* 159.3, pp. 157 –184. ISSN: 0010-4655. DOI: DOI:10.1016/j.cpc.2003.11.002. URL: http://www.sciencedirect.com/science/article/pii/S0010465504001109.

Park, Y S and A S Welander (2006). "Real-time determination of magnetic island location for neoclassical tearing mode control in DIII-D." In: *Plasma Physics and Controlled Fusion* 48.9, pp. 1447–1454. URL: http://stacks.iop.org/0741-3335/48/1447.

Peeters, A. G. (Dec. 2000). "The bootstrap current and its consequences." In: *Plasma Physics and Controlled Fusion* 42, B231–B242.

Pereverzev, G. V. and P.N. Yushmanov (2002). *ASTRA Automated System for TRansport Analysis in a Tokamak*. Tech. rep. 5/98. IPP Report.

Petty, C.C. et al. (2004a). "Complete suppression of the m = 2/ n = 1 neoclassical tearing mode using electron cyclotron current drive in DIII-D." In: *Nuclear Fusion* 44.2, pp. 243–251. URL: http://stacks.iop.org/0029-5515/44/243.

Petty, C.C. et al. (2004b). "Onset and suppression of 2/1 NTM in DIII-D." In: *Proceedings of the 20th International Conference on Fusion Energy, Villamoura (PT)*. EX/7-3.

Peysson, Y and J Decker (2008). *Report EUR-CEA-FC-1739*. Tech. rep. EURATOM-CEA.

Pfeiffer, W. W. et al. (Dec. 1980). *ONETWO: A computer code for modeling plasma transport in Tokamaks*. Tech. rep.

Pietrzyk, Z. A. et al. (2001). "Long-Pulse Improved Central Electron Confinement in the TCV Tokamak with Electron Cyclotron Heating and Current Drive." In: *Phys. Rev. Lett.* 86.8, pp. 1530–1533. DOI: 10.1103/PhysRevLett.86.1530.

Piras, F. (2011). Private communication.

Piras, F., J.-M. Moret, and J.X. Rossel (2010a). "Measurement of the magnetic field errors on TCV." In: *Fusion Engineering and Design* 85.5, pp. 739 –744. ISSN: 0920-3796. DOI: DOI:10.1016/j.fusengdes.2010.04.049. URL: http://www.sciencedirect.com/science/article/pii/S0920379610001900.

Piras, F. et al. (2010b). ""Snowflake" H Mode in a Tokamak Plasma." In: *Phys. Rev. Lett.* 105.15, p. 155003. DOI: 10.1103/PhysRevLett.105.155003.

Pironti, A. and M. Walker (2005). "Control of tokamak plasmas: introduction to a special section." In: *Control Systems, IEEE* 25.5, pp. 24 –29. ISSN: 1066-033X. DOI: 10.1109/MCS.2005.1512793.

— (2006). "Control of tokamak plasmas. II." In: *Control Systems, IEEE* 26.2, pp. 30 –31. ISSN: 1066-033X. DOI: 10.1109/MCS.2006.1615270.

Pitts, R. et al. (Mar. 2001). "Divertor geometry effects on detachment in TCV." In: *Journal of Nuclear Materials* 290, pp. 940–946. DOI: 10.1016/S0022-3115(00)00461-X.

Pitts, R. A. et al. (Oct. 2003). "ELM driven divertor target currents on TCV." In: *Nuclear Fusion* 43, pp. 1145–1166. DOI: 10.1088/0029-5515/43/10/017.

Pitts, R. A. et al. (June 2007). "Parallel SOL flow on TCV." In: *Journal of Nuclear Materials* 363, pp. 505–510. DOI: 10.1016/j.jnucmat.2006.12.065.

Pitzschke, Andreas (2011). "Pedestal Characteristics and MHD Stability of H-Mode Plasmas in TCV." PhD thesis. EPFL, Lausanne, Switzerland.

Pletzer, A., A. Bondeson, and R.L. Dewar (1994). "Linear Stabiliby of Resistive MHD modes: Axisymmetric Toroidal Computation of the Outer Region Matching Data." In: *Journal of Computational Physics* 115, pp. 530–549.

Pochelon, A. et al. (2001). "Plasma shape effects on sawtooth/internal kink stability and plasma shaping using electron cyclotron wave current profile tailoring in TCV." In: *Nuclear Fusion* 41.11, p. 1663. URL: http://stacks.iop.org/0029-5515/41/i=11/a=316.

Polevoi, A.R. et al. (2002). In: *Proceedings of the 19th International Conference on Fusion Energy, Lyon (FR)*. IAEA, Vienna, CT/P–08.

Poli, E., A. G. Peeters, and G. V. Pereverzev (2001). "TORBEAM, a beam tracing code for electron-cyclotron waves in tokamak plasmas." In: *Computer Physics Communications* 136.1-2, pp. 90 –104. ISSN: 0010-4655. DOI: DOI:10.1016/S0010-4655(01)00146-1. URL: http://www.sciencedirect.com/science/article/pii/S0010465501001461.

Poli, E. et al. (2002). "Reduction of the Ion Drive and ρ_θ^* Scaling of the Neoclassical Tearing Mode." In: *Phys. Rev. Lett.* 88.7, p. 075001. DOI: 10.1103/PhysRevLett.88.075001.

Popov, A. M. et al. (2002a). "Simulation of neoclassical tearing modes in the DIII-D tokamak. II. Suppression by radially localized electron cyclotron current drive." In: 9.10, pp. 4229–4240. ISSN: 1070664X. DOI: DOI:10.1063/1.1505843. URL: http://dx.doi.org/doi/10.1063/1.1505843.

— (2002b). "Simulation of neoclassical tearing modes (NTMs) in the DIII-D tokamak.I. NTM excitation." In: 9.10, pp. 4205–4228. ISSN: 1070664X. DOI: DOI:10.1063/1.1505842. URL: http://dx.doi.org/doi/10.1063/1.1505842.

Porcelli, F, D Boucher, and M N Rosenbluth (1996). "Model for the sawtooth period and amplitude." In: *Plasma Physics and Controlled Fusion* 38.12, pp. 2163–2186. URL: http://stacks.iop.org/0741-3335/38/2163.

Porte, L. et al. (Aug. 2007). "Plasma dynamics with second and third-harmonic ECRH and access to quasi-stationary ELM-free H-mode on TCV." In: *Nuclear Fusion* 47, pp. 952–960. DOI: 10.1088/0029-5515/47/8/029.

Prater, R. (2004). "Heating and current drive by electron cyclotron waves." In: *Physics of Plasmas* 11.5, pp. 2349–2376. DOI: 10.1063/1.1690762. URL: http://link.aip.org/link/?PHP/11/2349/1.

Prater, R. et al. (2007). "Stabilization and prevention of the 2/1 neoclassical tearing mode for improved performance in DIII-D." In: *Nuclear Fusion* 47.5, p. 371. URL: http://stacks.iop.org/0029-5515/47/i=5/a=001.

Press, William H. et al. (1996). *Numerical Recipes*. Second. New York: Cambridge University Press.

Raju, D (2011). Private communication.

Raju, D, O Sauter, and J B Lister (2003). "Study of nonlinear mode coupling during neoclassical tearing modes using bispectrum analysis." In: *Plasma Physics and Con-*

trolled Fusion 45.4, pp. 369–378. DOI: 10.1088/0741-3335/45/4/304. URL: http://stacks.iop.org/0741-3335/45/369.

Ramponi, G., E. Lazzaro, and S. Nowak (Sept. 1999). "On the stabilization of neoclassical tearing modes by electron cyclotron waves." In: *Physics of Plasmas* 6, pp. 3561–3570. DOI: 10.1063/1.873633.

Ramponi, G. et al. (2008). "Physics analysis of the ITER ECW system for optimized performance." In: *Nuclear Fusion* 48.5, p. 054012. URL: http://stacks.iop.org/0029-5515/48/i=5/a=054012.

Rattá, G.A. et al. (2010). "An advanced disruption predictor for JET tested in a simulated real-time environment." In: *Nuclear Fusion* 50.2, p. 025005. URL: http://stacks.iop.org/0029-5515/50/i=2/a=025005.

Rebut, P.H., P.P. Lallia, and M.L. Watkins (1989). In: *Plasma Physics and Controlled Nuclear Fusion Research 1988 (Proc. 12th Int. Conf. Nice, 1988)*. Vol. 2. IAEA, Vienna, p. 191.

Reimerdes, H. et al. (2002). "From Current-Driven to Neoclassically Driven Tearing Modes." In: *Phys. Rev. Lett.* 88.10, p. 105005. DOI: 10.1103/PhysRevLett.88.105005.

Reux, C. et al. (Sept. 2010). "Experimental study of disruption mitigation using massive injection of noble gases on Tore Supra." In: *Nuclear Fusion* 50.9, pp. 095006–+. DOI: 10.1088/0029-5515/50/9/095006.

Rossel, J et al. (2011). "Edge localized mode control by electron cyclotron waves in a Tokamak plasma." In: *Submitted to Physical Review Letters*.

Rutherford, P. H. (1973). "Nonlinear growth of the tearing mode." In: *Physics of Fluids* 16.11, pp. 1903–1908. DOI: 10.1063/1.1694232. URL: http://link.aip.org/link/?PFL/16/1903/1.

Ryutov, D D (1988). "Open-ended traps." In: *Soviet Physics Uspekhi* 31.4, p. 300. URL: http://stacks.iop.org/0038-5670/31/i=4/a=R02.

Sauter, O. et al. (1997). "Beta limits in long-pulse tokamak discharges." In: *Physics of Plasmas* 4.5, pp. 1654–1664. DOI: 10.1063/1.872270. URL: http://link.aip.org/link/?PHP/4/1654/1.

Sauter, O., C. Angioni, and Y. R. Lin-Liu (1999a). "Neoclassical conductivity and bootstrap current formulas for general axisymmetric equilibria and arbitrary collisionality regime." In: *Physics of Plasmas* 6.7, pp. 2834–2839. DOI: 10.1063/1.873240. URL: http://link.aip.org/link/?PHP/6/2834/1.

Sauter, O. et al. (1999b). "Sawtooth period simulations of TCV discharges." In: *Proc. Joint Varenna - Lausanne Int. Workshop on Theory of Fusion Plasmas Varenna, Italy, August 31 - September 4, 1998*. Vol. ISPP-18, pp. 403 –408.

Sauter, O. et al. (2001). "Steady-state fully noninductive operation with electron cyclotron current drive and current profile control in the tokamak à configuration variable (TCV)." In: 8.5, pp. 2199–2207. ISSN: 1070664X. DOI: DOI:10.1063/1.1355317. URL: http://dx.doi.org/doi/10.1063/1.1355317.

Sauter, O. et al. (2002a). "Control of Neoclassical Tearing Modes by Sawtooth Control." In: *Phys. Rev. Lett.* 88.10, p. 105001. DOI: 10.1103/PhysRevLett.88.105001.

Sauter, O et al. (2002b). "Marginal β -limit for neoclassical tearing modes in JET H-mode discharges." In: *Plasma Physics and Controlled Fusion* 44.9, pp. 1999–2019. DOI: 10.1088/0741-3335/44/9/315. URL: http://stacks.iop.org/0741-3335/44/1999.

Sauter, O. et al. (2005). "Inductive Current Density Perturbations to Probe Electron Internal Transport Barriers in Tokamaks." In: *Physical Review Letters* 94.10, 105002, p. 105002. DOI: 10.1103/PhysRevLett.94.105002. URL: http://link.aps.org/abstract/PRL/v94/e105002.

Sauter, O. et al. (Nov. 2010). "Experimental studies of ECRH/ECCD effects on Tearing Mode stability using the new TCV real-time control system." In: *APS Meeting Abstracts*, 9075P−+.

Sauter, O et al. (2010). "On the requirements to control neoclassical tearing modes in burning plasmas." In: *Plasma Physics and Controlled Fusion* 52.2, p. 025002. URL: http://stacks.iop.org/0741-3335/52/i=2/a=025002.

Scarabosio, A. et al. (May 2006). "Toroidal plasma rotation in the TCV tokamak." In: *Plasma Physics and Controlled Fusion* 48, pp. 663–683. DOI: 10.1088/0741-3335/48/5/012.

Scarabosio, A, A Pochelon, and Y Martin (2007). "Plasma shape stabilization of current rise MHD instabilities in TCV." In: *Plasma Physics and Controlled Fusion* 49.7, p. 1041. URL: http://stacks.iop.org/0741-3335/49/i=7/a=007.

Schlatter, Christian (2009). "Turbulent ion heating in TCV tokamak plasmas. Turbulent ion heating in TCV tokamak plasmas. Turbulent ion heating in TCV tokamak plasmas. Turbulent ion heating in the TCV tokamak." PhD thesis. Lausanne, Switzerland: EPFL.

Sevillano, Goretti et al. (2011). "Observer-based real-time control for the poloidal beta of the plasma using diamagnetic measurements in Tokamak fusion reactors." In: *Proceedings of the 50th IEEE Conference on Decision and Control and European Control Conference, Orlando, FL, USA*.

Shafranov, V. D. (1958). "On Magnetohydrodynamical Equilibrium Configurations." In: *Soviet Journal of Experimental and Theoretical Physics* 6, pp. 545−+.

Shimada, M. et al. (2007). "Chapter 1: Overview and summary." In: *Nuclear Fusion* 47.6, S1. URL: http://stacks.iop.org/0029-5515/47/i=6/a=S01.

Silva, Miguel et al. (2011). "Fast polarizers installation for ECRH and ECE in TCV." In: *Fusion Engineering and Design* In Press, Corrected Proof, pp. –. ISSN: 0920-3796. DOI: DOI:10.1016/j.fusengdes.2011.01.043. URL: http://www.sciencedirect.com/science/article/pii/S092037961100055X.

Singer, C. E. et al. (1988). "Baldur: A one-dimensional plasma transport code." In: *Computer Physics Communications* 49.2, pp. 275 –398. ISSN: 0010-4655. DOI: DOI:10.1016/0010-4655(88)90012-4. URL: http://www.sciencedirect.com/science/article/pii/0010465588900124.

Sips, A C C et al. (2002). "Progress towards steady-state advanced scenarios in ASDEX Upgrade." In: *Plasma Physics and Controlled Fusion* 44.5A, A151. URL: http://stacks.iop.org/0741-3335/44/i=5A/a=311.

Sips, A. C. C. et al. (May 2005). "Advanced scenarios for ITER operation." In: *Plasma Physics and Controlled Fusion* 47.26, A260000–A40. DOI: 10.1088/0741-3335/47/5A/003. eprint: arXiv:physics/0410263.

Smyshlyaev, Andrey and Miroslav Krstic (2010). *Adaptive Control of Parabolic PDEs.* Princeton, NJ (USA): Princeton Univeristy Press.

Söldner, F X and the JET Team (1997). "Shear optimization experiments with current profile control on JET." In: *Plasma Physics and Controlled Fusion* 39.12B, B353. URL: http://stacks.iop.org/0741-3335/39/i=12B/a=027.

Sontag, Eduardo D. (1998). *Mathematical Control Theory.* second. Vol. 6. Texts in Applied Mathematics. New York (USA): Springer.

Sushkov, A. et al. (Feb. 2008). "High-resolution multiwire proportional soft x-ray diagnostic measurements on TCV." In: *Review of Scientific Instruments* 79.2, pp. 023506–+. DOI: 10.1063/1.2833822.

Suttrop, W. et al. (June 2011). "First Observation of Edge Localized Modes Mitigation with Resonant and Nonresonant Magnetic Perturbations in ASDEX Upgrade." In: *Physical Review Letters* 106.22, pp. 225004–+. DOI: 10.1103/PhysRevLett.106.225004.

Suzuki, T. et al. (2008). "Off-axis current drive and real-time control of current profile in JT-60U." In: *Nuclear Fusion* 48.4, p. 045002. URL: http://stacks.iop.org/0029-5515/48/i=4/a=045002.

Teo, K.L., C.J. Goh, and K.H. Wong (1991). *A unified computational approach to optimal control problems.* Pitman Monographs and Surveys in Pure and Applied Mathematics. John Wiley & Sons Inc.

Troyon, F. et al. (Jan. 1984). "MHD-Limits to Plasma Confinement." In: *Plasma Physics and Controlled Fusion* 26, pp. 209–215. DOI: 10.1088/0741-3335/26/1A/319.

Turco, F. and T.C. Luce (2010). "Impact of the current profile evolution on tearing stability of ITER demonstration discharges in DIII-D." In: *Nuclear Fusion* 50.9, p. 095010. URL: http://stacks.iop.org/0029-5515/50/i=9/a=095010.

Turri, G et al. (2008). "MHD as trigger of electron temperature oscillations in ECCD discharges in TCV." In: *Plasma Physics and Controlled Fusion* 50.6, 065010 (13pp). URL: http://stacks.iop.org/0741-3335/50/065010.

Udintsev, V. S. et al. (2007). "Recent Electron Cyclotron Emission Results on TCV." In: *Fusion Science and Technology* 52.2, pp. 161–168.

Udintsev, V S et al. (2008). "Global plasma oscillations in electron internal transport barriers in TCV." In: *Plasma Physics and Controlled Fusion* 50.12, 124052 (12pp). URL: http://stacks.iop.org/0741-3335/50/124052.

Volpe, F. A. G. et al. (2009). "Advanced techniques for neoclassical tearing mode control in DIII-D." In: *Physics of Plasmas* 16.10, 102502, p. 102502. DOI: 10.1063/1.3232325. URL: http://link.aip.org/link/?PHP/16/102502/1.

Waelbroeck, F. L., J. W. Connor, and H. R. Wilson (2001). "Finite Larmor-Radius Theory of Magnetic Island Evolution." In: *Phys. Rev. Lett.* 87.21, p. 215003. DOI: 10.1103/PhysRevLett.87.215003.

Wagner, F et al. (2010). "On the heating mix of ITER." In: *Plasma Physics and Controlled Fusion* 52.12, p. 124044. URL: http://stacks.iop.org/0741-3335/52/i=12/a=124044.

Waltz, R. E. et al. (1997). "A gyro-Landau-fluid transport model." In: *Physics of Plasmas* 4.7, pp. 2482–2496. DOI: 10.1063/1.872228. URL: http://link.aip.org/link/?PHP/4/2482/1.

Weisen, H. et al. (1997). "Effect of plasma shape on confinement and MHD behaviour in the TCV tokamak." In: *Nuclear Fusion* 37.12, p. 1741. URL: http://stacks.iop.org/0029-5515/37/i=12/a=I07.

Weisen, H. et al. (2002). "Shape dependence of sawtooth inversion radii and profile peaking factors in TCV L mode plasmas." In: *Nuclear Fusion* 42.2, p. 136. URL: http://stacks.iop.org/0029-5515/42/i=2/a=303.

Wesson, John (2004). *Tokamaks.* Third edition. Vol. 118. International series of monographs on physics. New York (USA): Oxford Science Publications. ISBN: 0-19-8509227.

Westerhof, E. (1990). "Tearing mode stabilization by local current density perturbations." In: *Nuclear Fusion* 30.6, pp. 1143–1147.

Westerhof, E. et al. (Nov. 2002). "Control of sawteeth and triggering of NTMs with ion cyclotron resonance frequency waves in JET." In: *Nuclear Fusion* 42, pp. 1324–1334. DOI: 10.1088/0029-5515/42/11/306.

Wijnands, T. et al. (June 1997). "Feedback control of the current profile on Tore Supra." In: *Nuclear Fusion* 37, pp. 777–791. DOI: 10.1088/0029-5515/37/6/I06.

Wilson, H. R. et al. (1996). "Threshold for neoclassical magnetic islands in a low collision frequency tokamak." In: *Physics of Plasmas* 3.1, pp. 248–265. ISSN: 1070664X. DOI: DOI:10.1063/1.871830.

Witrant, E et al. (2007). "A control-oriented model of the current profile in tokamak plasma." In: *Plasma Physics and Controlled Fusion* 49.7, pp. 1075–1105. URL: http://stacks.iop.org/0741-3335/49/1075.

Witvoet, G. et al. (2011). "Numerical demonstration of injection locking of the sawtooth period by means of modulated EC current drive." In: *Nuclear Fusion* 51.10, p. 103043. URL: http://stacks.iop.org/0029-5515/51/i=10/a=103043.

Witvoet, G. et al. (July 2011). "Systematic design of a sawtooth period feedback controller using a Kadomtsev-Porcelli sawtooth model." In: *Nuclear Fusion* 51.7, pp. 073024–+. DOI: 10.1088/0029-5515/51/7/073024.

Xu, C. et al. (2010a). "Ramp-Up-Phase Current-Profile Control of Tokamak Plasmas via Nonlinear Programming." In: *Plasma Science, IEEE Transactions on* 38.2, pp. 163 –173. ISSN: 0093-3813. DOI: 10.1109/TPS.2009.2037626.

Xu, Chao, Yongsheng Ou, and E. Schuster (2010b). "Transport Parameter Estimations of Plasma Transport Dynamics Using the Extended Kalman Filter." In: *Plasma Science, IEEE Transactions on* 38.3, pp. 359 –364. ISSN: 0093-3813. DOI: 10.1109/TPS.2009.2038220.

Zeeland, M.A. Van et al. (2008). "Tearing mode structure in the DIII-D tokamak through spectrally filtered fast visible bremsstrahlung imaging." In: *Nuclear Fusion* 48.9, p. 092002. URL: http://stacks.iop.org/0029-5515/48/i=9/a=092002.

Zhang, Y. et al. (June 2011). "Prediction of disruptions on ASDEX Upgrade using discriminant analysis." In: *Nuclear Fusion* 51.6, pp. 063039–+. DOI: 10.1088/0029-5515/51/6/063039.

Zohm, H. (2006). "The physics base for NTM stabilisation by ECCD in ITER." In: *14th Workshop on ECE and ECRH Santorini, Greece.*

Zohm, H. et al. (1999). "Experiments on neoclassical tearing mode stabilization by ECCD in ASDEX Upgrade." In: *Nuclear Fusion* 39.5, p. 577. URL: http://stacks.iop.org/0029-5515/39/i=5/a=101.

Zohm, H. et al. (2007). "Control of MHD instabilities by ECCD: ASDEX Upgrade results and implications for ITER." In: *Nuclear Fusion* 47.3, pp. 228–232. DOI: 10.1088/0029-5515/47/3/010. URL: http://stacks.iop.org/0029-5515/47/228.

Zucca, C et al. (2009a). "Current density evolution in electron internal transport barrier discharges in TCV." In: *Plasma Physics and Controlled Fusion* 51.1, 015002 (16pp). URL: http://stacks.iop.org/0741-3335/51/015002.

Zucca, C et al. (2009b). "Modulation of electron transport during swing ECCD discharges in TCV." In: *Plasma Physics and Controlled Fusion* 51.12, p. 125009. URL: http://stacks.iop.org/0741-3335/51/i=12/a=125009.

Zucca, Costanza (2009). "Modeling and control of the current density profile in tokamaks and its relation to electron transport." PhD thesis. EPFL, Lausanne, Switzerland.

Curriculum Vitae
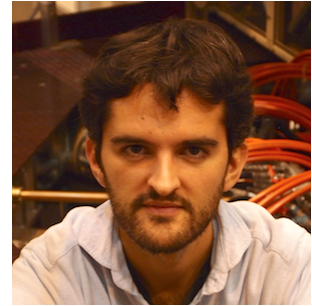
Federico Felici

PERSONAL

- Full name: Federico Alberto Alfredo FELICI
- Born: 17th May 1982 in Leiden (The Netherlands)
- Nationality: Italian and Dutch
- E-mail: ffelici@gmail.com

EDUCATION

École Polytechnique Fédérale de Lausanne (EPFL), Switzerland

Ph.D., Plasma Physics   2007-2011
Centre des Recherches en Physique des Plasmas (CRPP)

- Thesis Topic: *Real-time control of tokamak plasmas*
- Advisers: Dr. O. Sauter and Dr. T.P. Goodman
- Areas of study: Plasma physics, tokamak physics and control, plasma control using EC systems, MHD control, profile control, plasma transport simulations, real-time simulations, optimal control, EC polarization control.
- Several visits to the National Institute for Fusion Science (Japan) for research collaboration on feedback control of EC systems on the Large Helical Device.

Technische Universiteit Delft, The Netherlands

MSc., Systems & Control (*Cum Laude*)   2003-2005
Delft Center for Systems & Control

- Thesis Topic: *Subspace identification of LPV systems*
- Adviser: Prof. M. Verhaegen
- Areas of study: Control systems, system identification, intelligent control, model predictive control, robust control, optimal control, neural networks.
- Exchange year to Università di Bologna, Italy (Erasmus programme, 2003-2004)

BSc., Aerospace engineering (*Cum Laude*)   1999-2003

Het Rijnlands Lyceum Oegstgeest, The Netherlands

High School   1994-1999

- Subjects: Dutch, English, Math, Physics, Chemistry, Economics, Latin, Greek
- International Baccalaureate A2 English Second Language exam

OTHER RESEARCH
EXPERIENCE

Visiting researcher   Sep. – Dec. 2006
IDSIA institute for Artificial Intelligence, Lugano, Switzerland
- Adviser: Prof. J. Schmidhuber
- Area of Study: *Recurrent neural networks for time-series identification.*

Assistant Researcher   Dec. 2005 – Jun. 2006
Delft Center for Systems and Control
- Supervisor: Prof. M. Verhaegen
- Area of study: *Subspace identification of LPV systems using periodic scheduling sequences*

GRADUATE LEVEL
COURSES

- Physics of Magnetically confined plasmas
- Advanced theory of plasma
- Advanced topics in Numerical Modeling for PDEs
- The economics of technology policy
- Nonlinear control (L. Marconi, Università di Bologna, 2004)
- Identification and control of LPV systems (DISC summer school, 2006)

HONORS AND
AWARDS

- EPFL prize for dedication to teaching assistant duties (2009)
- VSB Fonds: 4000€ grant for 4-month post-master research stay at IDSIA.
- Nominated finalist for "KIVI-NIRIA Regeltechniek prijs" 2006 (Prize for best MSc thesis in control engineering)
- Nominated finalist for best junior presentation award, 25th Benelux Meeting on Systems & Control (2006)
- High school award for best results in science subjects (1999).

TEACHING
EXPERIENCE

Teaching assistant for several EPFL BSc. and MSc. classes. Responsible for preparation of exercises and solutions, assistant during exercise sessions.
- General Physics I, II
- Plasma Physics I (Dr. S. Alberti, 3rd year BSc. Physics)
- Nuclear Fusion and Plasma Physics (Prof. A. Fasoli and Prof. M.Q. Tran, 1st year MSc. Nuclear Engineering)

SKILLS

- Proficient in MATLAB and SIMULINK including several toolboxes.
- Good knowledge of LabView, C, Linux/UNIX, InDesign, MediaWiki, LATEX.
- Good knowledge of real-time signal processing software and hardware concepts, control systems technology.

LANGUAGES

- Italian and Dutch: Native speaker (bilingual)
- English: Fluent in speech and writing
- French: Fluent in speech, excellent writing

ACTIVITIES

- Initiative for reinstating regular PhD student seminars at CRPP (2010)
- Member of local organizing committee of the IAEA Fusion Energy Conference in Geneva, responsible for exposition by ITER domestic agencies (2008).
- Co-developer of new internal wiki page for CRPP. Now routinely used as main exchange platform for internal information including the TCV experiment (2007)
- Active member of student organization Augustinus in Leiden. Several leading positions in committees for 1500 member student organisation (2000-2006)

SELECTED
REFEREED
JOURNAL
PUBLICATIONS

- F. Felici, O. Sauter, S. Coda, et al. (2011b). "Real-time physics-model-based simulation of the current density profile in tokamak plasmas". In: *Nuclear Fusion* 51.8, p. 083052. URL: http://stacks.iop.org/0029-5515/51/i=8/a=083052

- T. P. Goodman, F. Felici, O. Sauter, et al. (June 2011). "Sawtooth Pacing by Real-Time Auxiliary Power Control in a Tokamak Plasma". In: *Physical Review Letters* 106.24, pp. 245002–+. DOI: 10.1103/PhysRevLett.106.245002

- M. Lauret, F. Felici, G. Witvoet, et al. (2011). "Demonstration of sawtooth period locking with power modulation in TCV plasmas". In: *Submitted to Physical Review Letters*

- F. Felici and O. Sauter (2011). "Nonlinear model-based optimization of actuator trajectories for tokamak plasma profile control". In: *Submitted to Plasma Physics and Controlled Fusion*

- F. Felici, T. Shimozuma, S. Kubo, et al. (Oct. 2010). "Feedback control of ECRH polarization on LHD". In: *Nuclear Fusion* 50.10, pp. 105003–+. DOI: 10.1088/0029-5515/50/10/105003

- F. Felici, T. Goodman, O. Sauter, et al. (2009). "Real-time feedback control of millimeter-wave polarization for LHD". In: *Review of Scientific Instruments* 80.1, p. 013504. DOI: 10.1063/1.3073735

- F. Felici, J-W. van Wingerden, and M. Verhaegen (2007). "Subspace identification of MIMO LPV systems using a periodic scheduling sequence". In: *Automatica* 43.10, pp. 1684 –1697. ISSN: 0005-1098. DOI: 10.1016/j.automatica.2007.02.027

SELECTED
CONFERENCE
PRESENTATIONS

- F. Felici, O. Sauter, S. Coda, et al. (2011a). "Optimization, real-time simulation and feedback control of tokamak plasma profiles on TCV". In: *38th EPS Conference on Plasma Physics, 27 June - 1 July, Strasbourg, France* (Oral presentation)

- F. Felici, O. Sauter, T. Goodman, et al. (Nov. 2010). "RAPTOR: Optimization, real-time simulation and control of the tokamak q profile evolution using a simplified transport model". In: *APS Meeting Abstracts*, 9090P–+ (Poster presentation)

- O. Sauter, F. Felici, T. Goodman, et al. (Nov. 2010). "Experimental studies of ECRH/ECCD effects on Tearing Mode stability using the new TCV real-time control system". In: *APS Meeting Abstracts*, 9075P–+ (Poster presentation)

- F. Felici, O. Sauter, T.P. Goodman, et al. (2009). "Self-consistent simulation of tearing modes during ECCD experiments on TCV". In: *36th EPS Conference on Plasma Physics, Sofia, Bulgaria, 29 June - 03 July* (Poster presentation)

- F. Felici, E. Asp, S. Cirant, et al. (2009). "Recent results of ECRH/ECCD experiments on TCV". In: *18th International Toki Conference, Gifu, Japan* (Oral presentation)

- F. Felici, C. Zucca, T.P Goodman, et al. (2008). "Safety factor profile influence on tearing mode stability in TCV". In: *Swiss Physical Society Annual Meeting, Geneva* (Oral presentation)

- Federico Felici, Jan-Willem van Wingerden, and Michel Verhaegen (2007). "Dedicated periodic scheduling sequences for LPV system identification". In: *European Control Conference, Kos, Greece* (Oral presentation)

A more extensive publication list can be found on http://people.epfl.ch/federico.felici